MANGO: A novel optimization model for the long-term, multi-stage planning of decentralized multi-energy systems

Journal Article

Author(s):
Mavromatidis, Georgios (ID); Petkov, Ivalin (ID)
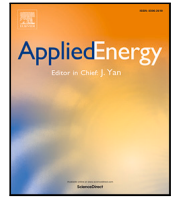
MANGO: A novel optimization model for the long-term, multi-stage planning of decentralized multi-energy systems

Georgios Mavromatidis *, Ivalin Petkov

Group for Sustainability and Technology, ETH Zurich, 8092 Zurich, Switzerland

ABSTRACT

This study presents MANGO (Multi-stAge eNerGy Optimization), a novel optimization model that incorporates a multi-year planning horizon, along with flexible, multi-stage investment strategies for the effective, long-term design of decentralized multi-energy systems (D-MES). By considering the dynamic surrounding energy and techno-economic landscape that evolves over time, MANGO harnesses the strategic value of investment flexibility and can optimally phase D-MES investments in order to benefit, for instance, from projected future reduced technology costs and technical improvements. To achieve this, the model considers the most relevant dynamic aspects, such as year-to-year variations in energy demands, changing energy carrier and technology prices, technical improvements and equipment degradation. MANGO is also capable of optimizing the design of complex configurations composed of multiple, interconnected D-MES installed at different locations. Finally, the model's formulation also addresses end-of-horizon effects that can distort solutions in multi-stage energy system models.

Besides presenting the key aspects and the mathematical formulation of MANGO, this study also uses the model to develop a six-stage energy design plan, along a 30-year project horizon, for an urban district composed of 3 sites in Zurich, Switzerland. One candidate D-MES is considered per site and different scenarios are examined regarding building retrofitting and D-MES interconnections. Results overall show that retrofitting leads to lower emission levels, but significantly higher costs. On the other hand, D-MES interconnections improve both the economic and the environmental system performance. Finally, regarding optimal D-MES configurations, a variety of technologies is used, with combinations of air-source heat pumps and natural gas boilers leading to better economic performance and combinations of ground-source heat pumps and biomass boilers to more environmentally-friendly designs.

Overall, MANGO facilitates D-MES decision-making at the strategic level by delivering flexible multi-stage investment strategies, at the economic level by providing detailed information about the systems' economic performance during each project year and, finally, at the technical level by specifying the optimal technical configurations of each D-MES and their optimal operating schedules. With its long-term perspective, MANGO can offer insights that closely match the dynamic class of real-world energy system design projects led by energy developers.

1. Introduction

1.1. Background: single- and multi-stage D-MES design

In response to contemporary energy challenges, decentralized multi-energy systems (D-MES) have the potential to secure the sustainable energy supply for existing and new buildings and districts [1]. D-MES typically integrate multiple conversion and storage technologies and use different energy networks to satisfy different types of energy demands (*e.g. thermal, electrical etc.*) for various consumer types. As a

result, D-MES can increase the utilization of local renewable energy [1], reduce the carbon intensity of energy supply [2], and even unlock new business opportunities [3,4].

D-MES design projects are commonly categorized based on their setting (urban, semi-urban, rural), spatial scale (single building, neighborhood, district) and application type (residential, commercial, industrial, mixed-use) [5–7]. In this work, we define two further classes of D-MES design projects based on the investment strategy that they consider,

namely *static* (or *single-stage*) and *dynamic* (or *multi-stage*) D-MES design projects.

We define the static class to include D-MES design projects that are characterized by a single, '*here-and-now*' investment at the beginning of the project without the possibility of additional investments during the system's lifetime. We refer to this D-MES design scheme as static because it is best suited for projects that do not include long-term developments to which the energy developer would need to react with additional investments.

In contrast to the static class, we label a D-MES design project as dynamic when it involves investment decisions in multiple stages during the project lifetime. The multi-stage investment strategy may be necessitated by specific project details, for instance, by long-term structural & developmental changes to a district with existing buildings being retrofitted and/or new buildings being added in multiple future phases. Additionally, a dynamic, multi-stage D-MES design scheme might also stem from the developer's efforts to harness the value of investment flexibility. By investment flexibility, we refer to the influence of developments in the surrounding economic and energy landscape on optimally phased investment strategies, in order to benefit from projected future technological improvements, cost reductions, and energy carrier price changes, among others.

A certain overlap can be noted between single- and multi-stage D-MES design projects, most notably regarding decisions pertaining to the selection and siting of technologies that need to be installed. Nevertheless, the addition of a temporal dimension in the decisions of multi-stage projects, regarding the *optimal timing* of the investments, introduces an additional layer of decision-making complexity and establishes them as a separate dynamic class of D-MES design projects.

1.2. Literature review

The largest body of D-MES literature has focused on single-stage D-MES design projects. Multiple studies have presented models that are based on optimization techniques like Mixed-Integer Linear Programming (MILP) and aim to simultaneously optimize the single-stage D-MES design and its operating strategy. To calculate the system's operation, the most common approach is to use a single, representative year, and extrapolate the results over the lifetime of the D-MES (see *e.g.* [8–10]). The use of a representative year reduces the data requirements for the analysis; however, the inherent assumption in this practice is that all relevant parameters for the design (energy demands, techno-economic parameters etc.) will stay constant at their assumed values during the project lifetime, which can in turn lead to sub-optimal decisions. As a result, some studies have combined single-stage investment decisions with multi-year analyses of D-MES operation *e.g.* in order to account for changing energy demands due to climate change [11] or for changing energy carrier prices [12]. The potential of these single-stage D-MES design models has been illustrated with case studies across different scales and settings, including rural communities [13], urban districts [14], industrial clusters [15], and university campuses [16]. Finally, several recent studies have developed advanced model features, including modeling of seasonal storage technologies [17,18], the concurrent optimization of building geometries and D-MES design [19], demand shifting to times of lower grid carbon intensity by considering time-varying electricity grid emission factors [20], and, finally, the ability to investigate the impact of uncertainty on single-stage D-MES design [10,21].

On the other hand, the dynamic class of multi-stage D-MES design problems has been mostly overlooked in the literature. A simplified approach to approximate multi-stage D-MES design includes using a single-stage model and solving it sequentially for multiple future years/stages with the corresponding future values for the input parameters. Murray et al. [22], for instance, used a static single-stage D-MES design model to identify optimal D-MES designs for one urban and one rural neighborhood in Switzerland for the years 2015, 2020, 2035, and 2050. The advantage of this approach is that a readily available, single-stage D-MES design model can be used to approximate a multi-stage energy plan. Its disadvantage, however, is that it is a myopic approach with the D-MES design for each stage being optimized independently from all other preceding and subsequent stages. As a result, the continuity of the energy system is not considered and the possibility of, for instance, postponing technology investments to a later stage cannot be evaluated.

An alternative option would be to use models like TIMES [23–25] or OSeMOSYS [26], which incorporate multi-stage investment decisions and, although their primary focus is on national energy system planning, can also be applied for local energy systems *e.g.* at the community level. Nevertheless, some of their characteristics prevent them from being readily or easily applied for D-MES design applications. One such important characteristic is, for instance, the aggregated representation of a whole city or community into a single energy entity, when D-MES models typically exhibit high spatial resolution down to building-level representations [27]. As a result, although studies that have used the TIMES model to create strategies for urban and community energy systems can provide valuable strategic insights (see *e.g.* [28,29]), their aggregated view of the energy system means that the results cannot be used to precisely plan the multi-stage design of a D-MES.

In order to address these issues, in the recent years, some studies have presented models developed specifically for the optimal, multi-stage design of D-MES. Cano et al. [30] presented a model that can output a multi-year investment plan for an energy system taking into account future energy costs and energy demands, as well as aspects like technology aging. In a similar direction, Pecenak et al. [31] presented a model for the multi-year planning of microgrids. Their model considers the future evolution of energy carrier and technology prices, energy demands, as well as technology degradation. Wei et al. [32] presented a model for the multi-stage design of multi-energy microgrids, which can also consider the influence of short- and long-term uncertainty for more robust designs. Finally, in a more recent study, Faraji et al. [33] combined long-term load forecasting using artificial neural networks (ANNs) with the multi-year module of the HOMER software [34] for the multi-stage design of a microgrid in Iran.

These studies form important contributions towards establishing methodologies for the dynamic multi-stage design of D-MES. However, there remain some issues that need to be addressed. First, neither of the models consider technological improvements over the planning horizon, which could, for instance, change the efficiency of technologies that still experience techno-economic learning, and in turn change the optimal investment decisions. As a result, since all investments in one technology have the same technical characteristics in the model, their capacities are aggregated and their operation is calculated as if they were one single unit. Nevertheless, taking into account the projected technological improvements for less mature technologies could uncover better future investment opportunities. Therefore, it would be important for the model to include such capabilities and to be able to evaluate their influence by tracking the different installations and calculating their operation as distinct units.

Second, neither of these studies address the end-of-horizon effects that are known to distort the solutions in long-term, multi-stage energy models [35]. These effects are a consequence of the models' finite planning horizon and they pertain to penalizing investments towards the end of the model's horizon, which are fully paid, but their benefit (*i.e.* operating during their lifetime) is not fully realized. This effect can distort these later investment decisions (*e.g.* by favoring less capital intensive technologies), but also influence decisions in earlier stages, since they are made in anticipation of developments in the future. The longer the model horizon, the less significant these effects become; nevertheless, it is important to mitigate these end-of-horizon effects for more effective D-MES investment decisions.

Third, the models by Cano et al., Pecenak et al., and Faraji et al. are only capable of optimizing single D-MES installations, but not multiple, spatially distributed and interconnected D-MES installations. In recent years, multiple studies from the single-stage D-MES design literature have demonstrated the benefits of considering multiple D-MES capable of exchanging energy with each other, especially at larger spatial scales (*e.g.* [16,27,36,37]). Interconnections between D-MES can lead to an overall energy system that is able to achieve reduced system costs and emissions, for instance, due to smoother demand profiles and smaller overall capacities due to technology sharing. Thus, the consideration of multiple interconnected D-MES is an important aspect that multi-stage D-MES design models should also be able to address. The model by Wei et al. does include multi-location optimization capabilities; however, the authors in the paper do not demonstrate these capabilities, as the illustrative case study used is for a single-location system.

As a final point, beyond the models' capabilities, we argue that for different reasons these previous studies have not fully demonstrated the advantages of multi-stage design processes for D-MES and the insights that they can provide for D-MES developers. For instance, Cano et al. consider only a single technology (photovoltaic (PV) panels) for the different stages. Pecenak et al. placed the main focus of the study on comparing the multi-stage D-MES design methodology with an adaptive method that uses a sequence of single-year optimizations to approximate multi-stage decisions. In the study by Wei et al. the focus is placed on comparing combined heat and electricity supply planning to separated planning, the impact of battery price developments and the computational efficiency of their proposed method. Finally, Faraji et al. focus primarily on different methods to project the multi-year load growth.

1.3. This paper

In summary, previous studies that dealt with the multi-stage design of D-MES (i) did not include the option for considering future technological improvements in the model, (ii) did not address end-of-horizon effects, (iii) did not optimize the design of multi-location D-MES configurations, and (iv) did not sufficiently highlight the results and value of dynamic multi-stage D-MES design. With this paper, we address these methodological and knowledge gaps and contribute to the nascent field of multi-stage D-MES design with the introduction of our novel Multi-stAge eNerGy Optimization (MANGO) model. The paper's main contributions are summarized as follows:

- The development of a state-of-the-art optimization model for D-MES design that incorporates a multi-year horizon, is capable of considering flexible, multi-stage investment strategies and can optimize the design of complex configurations composed of multiple, interconnected D-MES. The model's formulation enables the representation of finite planning horizons of any length, while also mitigating end-of-horizon effects.
- The consideration in the model of the most relevant dynamic aspects and parameters that evolve during the multi-year planning horizon, including year-to-year variations in energy demands, changing energy carrier prices and technology costs, technical improvements for conversion and storage technologies and equipment degradation.
- The application of the model to a dynamic urban district case study development (existing and new buildings) to illustrate the model's application and to highlight the insights that it can offer to developers dealing with real-world multi-stage D-MES design tasks.

This paper is structured as follows: Section 2 describes the main features and the formulation of the optimization model for multi-stage, interconnected D-MES design. Section 3 introduces the case study that is used to illustrate the main outputs of the model and the insights that it can generate. Section 4 presents the results of the paper. Finally, in Section 5, the paper's concluding remarks are given.

2. MANGO: A model for the optimal, multi-stage design of D-MES

This section introduces MANGO, a model to identify optimal multi-stage design solutions and operating strategies for one or more D-MES according to economic and environmental objectives. The key characteristics and the mathematical formulation of the most important elements of MANGO are presented here; the complete model formulation and detailed explanation of all parameters, variables, constraints and objective functions are provided in Appendix A. Overall, all model constraints and objective functions are linear, with both continuous and integer (binary) variables included. Hence, the developed model is formulated as a MILP, which means it can be solved very efficiently with state-of-the-art MILP solvers like Gurobi [38] or CPLEX [39].

2.1. Key MANGO model aspects

2.1.1. Multi-year horizon and long-term dynamic aspects

Starting from MANGO's temporal dimension, the model's horizon is composed of multiple years $y \in \mathcal{Y}$ to include a long-term perspective for the D-MES design task. Each year is represented with a set of days $d \in D$, each of which is in turn composed of individual time steps $t \in \mathcal{T}$. These relationships between years y, days d and hourly time steps t is depicted graphically in Fig. 1. The set D can include every day of each year y in the model horizon. However, in order to reduce the model's computational requirements, a number of typical days is used instead to represent the complete set of days in a year.[1]

In order for multi-stage D-MES planning to harness the value of flexible investment decisions, it needs to capture the long-term, dynamic developments in the surrounding economic and energy landscape that influence the D-MES design and operation decisions. In MANGO, the following aspects are considered as dynamic and evolving during the model's multi-year horizon:

- The annual energy demands and renewable availability levels[2]
- The energy carrier prices and emission factors[3]
- The conversion and storage technology costs and technological improvements regarding conversion efficiencies and energy storage performance[4]
- Technology degradation leading to deteriorating energy performance of installed equipment based on its age[5]

2.1.2. Multi-stage investment strategy

Next, we introduce the multi-stage investment strategies considered in the MANGO model. The simplest approach to achieve this would be to allow investments to happen at the beginning of each year y in the model horizon. However, in many real-world projects with long lifetimes (*e.g.* 30 years or longer), investments might be considered only for a small number of stages, which are usually defined by the specific project details. While considering more investment stages will result in a more flexible D-MES design plan, it also increases the plan's complexity, which can be a limitation for real-world projects.

Hence, to introduce some flexibility in the model, we decouple the model's investment stages $w \in \mathcal{W}$ from the years $y \in \mathcal{Y}$ in the model horizon, with $\mathcal{W} \subseteq \mathcal{Y}$, which means that the model is able to accommodate any multi-stage investment configuration with an arbitrary number and frequency of investment stages.

---

[1] By increasing the number of typical days to 365, a whole calendar year can also be represented in the model.

[2] Energy demands and renewable availability levels are still expressed with a time step resolution in the model.

[3] Energy carrier prices and emission factors vary per year but are assumed constant during each year.

[4] Technology costs and technical characteristics are assumed to change at an annual resolution.

[5] Degradation is assumed to occur per year based on the technology's age.
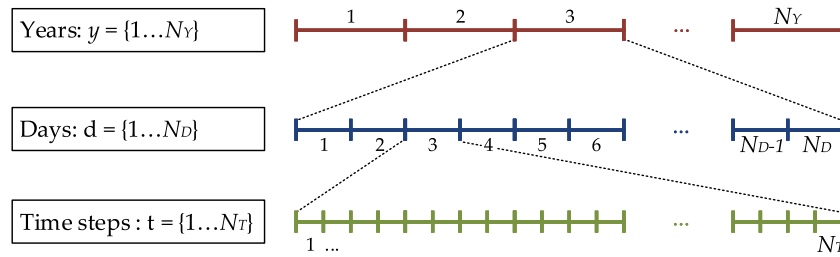
Fig. 1. Temporal horizon representation in the MANGO model using a sequence of years, days, and time steps.
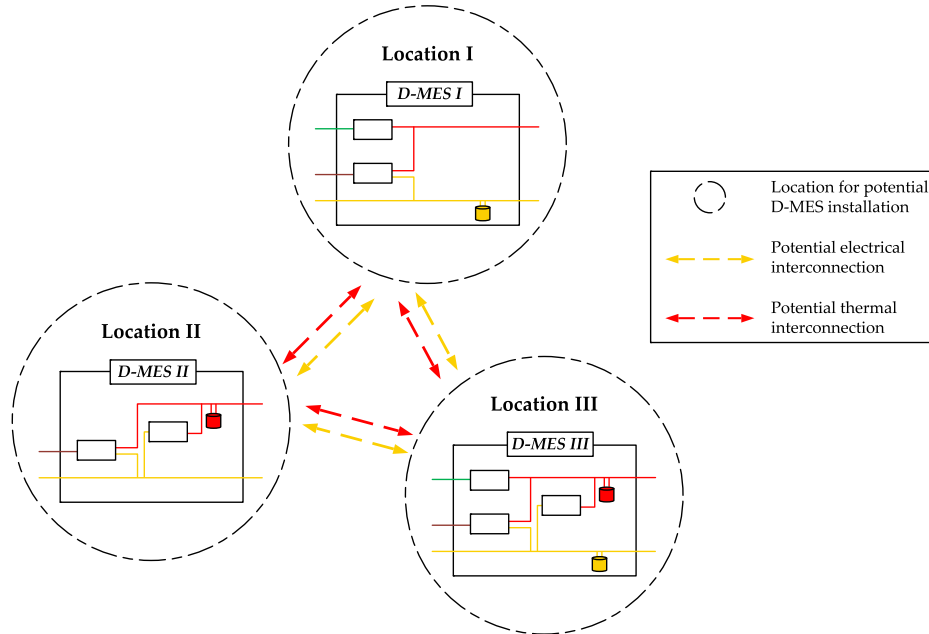

Fig. 2. Conceptual representation of multiple, interconnected D-MES exchanging energy with each other.

2.1.3. Multi-location D-MES configurations

An explicit spatial dimension is also included in the model. More specifically, MANGO can consider multiple locations $l \in \mathcal{L}$, with each one representing one or more energy consumers, whose energy demands need to be met. MANGO is then capable to design energy systems deciding among the following options:

- One D-MES installed at each location with no interconnections between them
- One D-MES installed at each location with possible interconnections between them
- D-MES installed at one or more locations serving end-users at other locations through interconnections

The concept of multi-location D-MES configurations is illustrated graphically in Fig. 2.

2.1.4. Multi-stage D-MES design task

The final aspect to be discussed is MANGO's multi-stage D-MES design task. For a given design problem, first, the candidate energy conversion ($c \in C$) and storage ($s \in S$) technologies that can be used to compose a D-MES need to be defined, along with the energy carriers ($ec \in \mathcal{EC}$) that can be imported, converted, stored or exported by a D-MES, consumed by the energy consumers, or exchanged between multiple D-MES. Then, the objective(s) according to which the design needs to be optimized must be specified. MANGO includes economic (minimization of total system cost) and environmental (minimization of total system CO_2 emissions) objectives, since ensuring affordable

and sustainable energy supply are two of the most important driving factors behind the adoption of D-MES. Nevertheless, MANGO can also accommodate any other types of objectives used in energy system optimization models such as maximizing reliability, renewables integration etc. [40,41].

Given the candidate technologies, the energy carriers in the system, and the objective functions to be optimized, MANGO makes design decisions regarding *what, where and when* actions. More specifically, regarding conversion and storage technologies, the model identifies which ones need to be installed and what their capacities should be (what), at which location they need to be placed (where), and at which investment stage they need to be installed (when). Finally, regarding D-MES interconnections, the model decides if they need to be established (what), between which locations (where) and at which investment stage (when). Since design decisions are also influenced by the energy system operation, the model also identifies the optimal operation for the technologies of each D-MES and the energy exchanges between them along the multi-year horizon $\mathcal{Y}$.

2.2. Optimization model formulation

Following the presentation of the key MANGO model aspects, this section discusses the key details of MANGO's mathematical formulation which are presented in more detail in Appendix A.

2.2.1. Sets

The various temporal, spatial and technological dimensions outlined for the model in the preceding section form the sets that are used in

MANGO to index the model parameters, variables, and constraints. Table 1 presents a summary of all model sets along with their description and also defines some useful subsets for the energy carrier set, $\mathcal{EC}$, and the conversion technology set, C.

2.2.2. Parameters

MANGO requires different parameters in order to perform the task of D-MES design. The main parameter categories include:

- Energy demand profiles that accurately reflect short-term variability and long-term developments
- Renewable energy availability profiles that accurately reflect short-term variability and long-term patterns
- Economic parameters, such as the evolution of energy carrier prices and technology costs, maintenance costs etc.
- Technical parameters pertaining to the operation and the performance of conversion, storage and network technologies, such as conversion efficiencies, self-discharge losses, network losses, technology lifetimes etc.
- Miscellaneous parameters connected to case-specific limitations or characteristics, such as the availability of roof area for solar technology installations

All model parameters, their mathematical notation and definition are discussed in more detail in Appendix A.2.

2.2.3. Decision variables

MANGO's decision variables are split into two groups, depending on whether they pertain to design or operational aspects of D-MES. The full list of D-MES design variables is given in Table A.5, but the most important ones are also discussed here:

- $NCAP^{conv}_{c,l,w}$: New capacity of conversion technology c, installed at location l, in investment stage w
- $NCAP^{stor}_{s,l,w}$: New capacity of storage technology of type s, installed at location l, in investment stage w
- $Y^{net}_{ec_x,l,l',w}$: Binary variable denoting the initial connection to exchange energy carrier ec_x, between energy system locations l, l', in investment stage w

The variables in the model pertaining to operating aspects of the D-MES are described as follows. Since they refer to D-MES operation, all variables are indexed per year y, day d, and hour t in addition to their specific indices discussed below:

- $P^{imp}_{ec_i,l,y,d,t}$: Import of energy carrier ec_i, at energy system location l
- $P^{conv}_{c,l,w,y,d,t}$: Input energy to conversion technology c, installed at energy system location l, in investment stage w[6]
- $P^{exp}_{ec_e,l,y,d,t}$: Exported energy of carrier ec_e, at energy system location l
- $P^{exc}_{ec_x,l,l',y,d,t}$: Exchanged energy of energy carrier ec_x, from location l to location l'
- $SoC_{s,l,w,y,d,t}$: State of charge of storage technology s, installed at energy system location l, in investment stage w[7]

- $Q^{ch}_{s,l,w,y,d,t}$: Charging energy into a storage technology s, installed at energy system location l, in investment stage w[7]
- $Q^{dis}_{s,l,w,y,d,t}$: Discharging energy out of a storage technology s, installed at energy system location l, in investment stage w[7]

2.2.4. Objective functions

As mentioned earlier, the minimization of the total energy system cost and of the total CO_2 emissions over the multi-year horizon are the two objectives integrated in the MANGO model.

The definition of the total cost T^{cost} is given in Eq. (1) and is composed of terms that represent the total investment expenditure, the total operating expenditure and the salvage value of the system at the end of the model horizon. The exact mathematical definitions of the individual terms in Eq. (1) are given in Appendix A.

$$\min T^{cost} = \underbrace{\sum_{l,w} \left(C^{INV,TECH}_{l,w} + C^{INV,NET}_{l,w} \right) \cdot \frac{1}{(1+r)^{w-1}}}_{\text{Investment expenditure}}$$
$$+ \underbrace{\sum_{l,y} \left(C^{IMP}_{l,y} + C^{MAINT}_{l,y} - R^{EXP}_{l,y} \right) \cdot \frac{1}{(1+r)^y}}_{\text{Operating expenditure}} \quad (1)$$
$$- \underbrace{\sum_{l} R^{SLVG}_l \cdot \frac{1}{(1+r)^{|\mathcal{Y}|+1}}}_{\text{Salvage value}}$$

The investment expenditure is composed of a sum over all energy system locations l and investment stages w of the individual expenditures for energy conversion and storage technologies, $C^{INV,TECH}_{l,w}$ and the expenditure for energy networks to interconnect individual D-MES, $C^{INV,NET}_{l,w}$. The operating expenditure is defined as the sum over all energy system locations l and years y of the individual expenditure due to energy carrier imports, $C^{IMP}_{l,y}$, technology maintenance, $C^{MAINT}_{l,y}$, and, the revenue due to energy carrier exports ($R^{EXP}_{l,y}$).

Finally, the salvage value is defined as the sum of the individual salvage value terms (R^{SLVG}_l). These terms represent the remaining value that is retained by technologies at location l that have not reached the end of their lifetime at the end of the model horizon. The salvage value is credited back to the total system cost to offset part of the investment costs in technologies that have been utilized only for a fraction of their lifetime in the model. Hence, the use of these salvage values can mitigate the distorting end-of-horizon effects discussed in the Introduction. The amount of salvage value depends on the investment stage a technology was installed, its operational lifetime and its initial investment cost (the exact definition of the R^{SLVG}_l is given in Eq. (A.12)). Technologies reaching the end of their lifetime during the modeled horizon are assumed to have no salvage value.

All terms of Eq. (1) are discounted to present values with the discount rate r. All investment expenditures are assumed to occur at the beginning of the year corresponding to each investment stage w, operating expenditures at the end of the year y, while the salvage value is paid back after the end of the model horizon.

The second objective function considered in the model, namely the total CO_2 emissions for the designed energy system, is expressed as the sum over all energy system locations l and years y of individual emission terms, $E^{CO_2}_{l,y}$, as shown in Eq. (2):

$$\min T^{CO_2} = \sum_{l,y} \left(E^{CO_2}_{l,y} \right) \quad (2)$$

The $E^{CO_2}_{l,y}$ term includes only operational CO_2 emissions and, more specifically, direct emissions due to local energy carrier utilization (e.g. fossil fuel combustion) and indirect emissions due to energy imports (e.g. grid electricity imports). The exact mathematical definitions of the $E^{CO_2}_{l,y}$ terms in is given in Appendix A.

---

[6] The definition domain for the variables $P^{conv}_{c,l,w,y,d,t}$ includes the conditions: $y \geq w$ and $y \leq w + cl_c - 1$, which defines the operating period of conversion technology c, with cl_c being the lifetime of the technology. This ensures that a technology cannot operate in the years before the investment stage it is installed and also that it cannot operate beyond its lifetime cl_c. For instance, if a technology is installed in stage $w = 1$ and has a lifetime of 15 years, it will be operational between $y \geq 1$ and $y \leq 15$.

[7] Similarly to the case of $P^{conv}_{c,l,w,y,d,t}$, the definition domains for the variables $SoC_{s,l,w,y,d,t}$, $Q^{ch}_{s,l,w,y,d,t}$, and $Q^{dis}_{s,l,w,y,d,t}$ include the conditions: $y \geq w$ and $y \leq w + sl_s - 1$, with sl_s being the lifetime of storage technology s, to ensure that operating variables are only defined for the operating period of the storage technology s.

Table 1
MANGO model sets and indices.

Set	Index	Description
$\mathcal{Y}$	y	Calendar years considered in the model horizon
$\mathcal{D}$	d	Set of representative days considered for each year
$\mathcal{T}$	t	Time steps considered for each day
$\mathcal{W} \subseteq \mathcal{Y}$	w	Investment stages
$\mathcal{L}$	l	Energy system locations
$\mathcal{EC}$	ec	All energy carriers in the energy system
$\mathcal{EC}_i \subseteq \mathcal{EC}$	ec_i	Energy carriers that can be imported by the energy system
$\mathcal{EC}_e \subseteq \mathcal{EC}$	ec_e	Energy carriers that can be exported from the energy system
$\mathcal{EC}_x \subseteq \mathcal{EC}$	ec_x	Energy carriers that can be exchanged between energy system locations
$\mathcal{EC}_d \subseteq \mathcal{EC}$	ec_d	Energy carriers for which demands are established
$\mathcal{C}$	c	Energy conversion technologies
$\mathcal{C}_{sol} \subseteq \mathcal{C}$	c_{sol}	Solar energy conversion technologies
$\mathcal{C}_d \subseteq \mathcal{C}$	c_d	Dispatchable energy conversion technologies
$\mathcal{S}$	s	Energy storage technologies

MANGO can be used in both single- and multi-objective optimization modes considering both the cost and CO_2 objective. In the latter case, the multi-objective problem is solved using the augmented ϵ-constraint method from [42], as it has been shown to avoid the production of weakly Pareto optimal solutions.

2.2.5. Constraints

The final necessary building block of an optimization model is the constraints that define balances, limitations, upper/lower bounds or minimum requirements involving the model's decision variables. In MANGO, constraints are needed to describe technical, physical and performance constraints that pertain to design and operating aspects of D-MES and they include:

- Energy balances for each D-MES to ensure that the energy demands of the end-users are met considering energy imports, conversion, storage, exports and exchanges between locations
- Energy balances for each energy storage system to describe the relationship between each storage's state-of-charge and charging and discharging energy flows
- Constraints preventing the generation and storage of energy beyond the installed technology capacities
- Constraints limiting storage charge/discharge rates to their maximum allowed values
- Physical resource limits, such as the roof area availability for solar technologies and the availability of biomass for energy applications
- Constraints that govern the interconnections between D-MES

In this section, the mathematical formulation of the energy balance constraints for each D-MES are presented in order to demonstrate how the model calculates the operating patterns of all technologies and to highlight some important model characteristics (the formulation of the rest of the MANGO constraints are presented in Appendix A).

The energy balance constraint is shown in Eq. (3). In broad terms, it states that the end-user energy demands, $dem_{ec_d,l,y,d,t}$, at location l, for energy carrier ec_d, must be balanced by energy imports, conversion, storage, exchange and exports for every year y, day d and time step t in the model horizon. Therefore, by applying it for all energy carriers ec and locations l, the model is able to calculate the optimal operation of the whole energy system across the complete model horizon.

In Eq. (3), apart from the model decision variables, which are described in Section 2.2.3, the following terms are included: $\eta_{c,ec,w}^{conv}$ is the conversion factor for technology c and energy carrier ec that is installed in stage w. $cdeg_{c,ec,w,y}$ is the total degradation coefficient for the conversion factor of technology c and energy carrier ec depending on the installation stage w and the operation year y. $stc_{s,ec}$ is a coupling parameter describing the energy carrier ec that can be stored in storage technology s. $\eta_{ec_x}^{net}$ is a term representing the loss factor per unit distance

of the network technology used to exchange energy carrier ec_x between locations. Finally, $x_{l,l'}$ is the distance between locations l and l'.

$$
\underbrace{dem_{ec_d,l,y,d,t}}_{\text{Demand}} = \underbrace{P_{ec_i,l,y,d,t}^{imp}}_{\text{Import}} + \underbrace{\sum_{\substack{c,w \\ y \geq w \\ y \leq w+cl_c-1}} \left(P_{c,l,w,y,d,t}^{conv} \cdot \eta_{c,ec,w}^{conv} \cdot cdeg_{c,ec,w,y} \right)}_{\text{Conversion}}
$$

$$
+ \underbrace{\sum_{\substack{s,w \\ y \geq w \\ y \leq w+sl_s-1}} \left[stc_{s,ec} \cdot (Q_{s,l,w,y,d,t}^{dis} - Q_{s,l,w,y,d,t}^{ch}) \right]}_{\text{Storage}}
$$

$$
+ \underbrace{\sum_{\substack{l,l' \\ l \neq l'}} \left[P_{ec_x,l',l,y,d,t}^{exc} \cdot (1 - \eta_{ec_x}^{net} \cdot x_{l',l}) - P_{ec_x,l,l',y,d,t}^{exc} \right]}_{\text{Exchange}} - \underbrace{P_{ec_e,l,y,d,t}^{exp}}_{\text{Export}},
$$

$$
\forall\ ec \in \mathcal{EC},\ l \in \mathcal{L},\ y \in \mathcal{Y},\ d \in \mathcal{D},\ t \in \mathcal{T}
$$

(3)

The constraint in Eq. (3) also serves to illustrate multiple key novel aspects of the model. The most important one is the separate dispatch of all installed conversion and storage technologies without aggregating them into one, 'virtual technology'. This is achieved by defining distinct energy conversion variables ($P_{c,l,w,y,d,t}^{conv}$) and storage variables ($Q_{s,l,w,y,d,t}^{dis}, Q_{s,l,w,y,d,t}^{ch}$) for the same technology type c but differentiating by the investment stage w when it was installed. This in turn enables the following novelties:

- *Technological improvements for conversion technologies*: The term $\eta_{c,ec,w}^{conv}$ allows the conversion efficiency of the same technology c to differ depending on the investment stage w when the technology is installed. This not only allows the model to optimize the investment timing, but combined with the separate dispatch aspect, to also separately optimize the operation schedule of each technology taking into account its nominal efficiency when installed.
- *Performance degradation for conversion technologies*: In a similar fashion to the previous aspect, the model is capable of tracking the degradation of the conversion efficiency of a technology c via the term $cdeg_{c,ec,w,y}$ and, via the separate dispatch, considering its impact on the operation of individual technologies.

2.3. Model summary and critical reflection

Overall, the MANGO model presented in this section can effectively perform the task of multi-stage D-MES design. The model integrates a multi-year horizon and is able to accommodate multi-stage strategies composed of any number and frequency of investment stages. Additionally, the model addresses the shortfalls of previous multi-stage

		Stage 1	Stage 2	Stage 3	Stage 4	Stage 5	Stage 6
Site	Development details	Phase 1 2021-2025	Phase 2 2026-2030	Phase 3 2031-2035	Phase 4 2036-2040	Phase 5 2041-2045	Phase 6 2046-2050
Site A	Existing mixed residential/commercial district: Building retrofitting ∣ 22'300 m²						
Site B	New residential development: 45 residential buildings ∣ 20'450 m²						
	New commercial development: 5 office buildings ∣ 17'200 m²						
Site C	New commercial development: 8 office buildings ∣ 25'300 m²						

Fig. 3. Investment stages, construction development phases and layout plan for the three sites of the case study urban development. In the timeline, dark colored sections signify construction/retrofit and operation phases, while lighter colored sections demonstrating solely operation.

design models, first, by including the option to consider technological improvements in the model; second, by using salvage values to mitigate end-of-horizon effects; and third, by optimizing the design of multi-location D-MES configurations.

However, these model innovations also introduce one important challenge. More specifically, the consideration of multi-location D-MES, as well as the separate tracking dispatch of each technology at each D-MES can increase significantly the number of variables in the model. As a result, although we have not performed any formalized comparisons and tests, we expect the computational requirements of MANGO to be higher compared to models that consider only single-location D-MES and aggregate all installed technologies of the same type into one, 'virtual' technology. Nevertheless, we argue that the benefits of these model additions outweigh the drawback of the increased computational costs, which will also get progressively lower with future advances in computing power and MILP solver technologies. In cases, though, when computational costs become prohibitive, reducing the resolution of the model horizon from single-year to multi-year (*e.g.* 5-year) increments will allow a reduction in computational costs, while also maintaining the MANGO model innovations.

Finally, a key characteristic of the MANGO model is its deterministic nature, meaning that perfect knowledge is assumed for all relevant model parameters. While the majority of the D-MES design models are also of deterministic nature, it can be argued that achieving full

certainty is nearly impossible, especially when such long-term decisions are to be made. From a modeling perspective, techniques like Stochastic Programming [43] are established approaches to deal with optimization under uncertainty and they have been successfully used in the past with single-stage D-MES models (see *e.g.* [44]). However, in order to incorporate uncertainty, these techniques lead to significant increases in computational cost requirements, which with MANGO and its multi-year, multi-location perspectives already has a considerably higher computational cost compared to single-stage D-MES. With this paper, our primary aim was to present a model that is capable of multi-stage D-MES design taking into account all relevant dynamic aspects, discuss the model's methodological details, and illustrate its value. Given the issue of increased computational requirements, if we were to formulate MANGO as a multi-stage stochastic optimization model, adjustments and simplifications would be necessary to ensure that it can be solved with reasonable computational effort, which would itself require a separate investigation. Therefore, we have opted to leave such an uncertainty investigation for future studies.

3. Illustrative case study

3.1. Case study composition

To demonstrate the model's application and the type of results and insights that it can generate, we investigate the multi-stage design
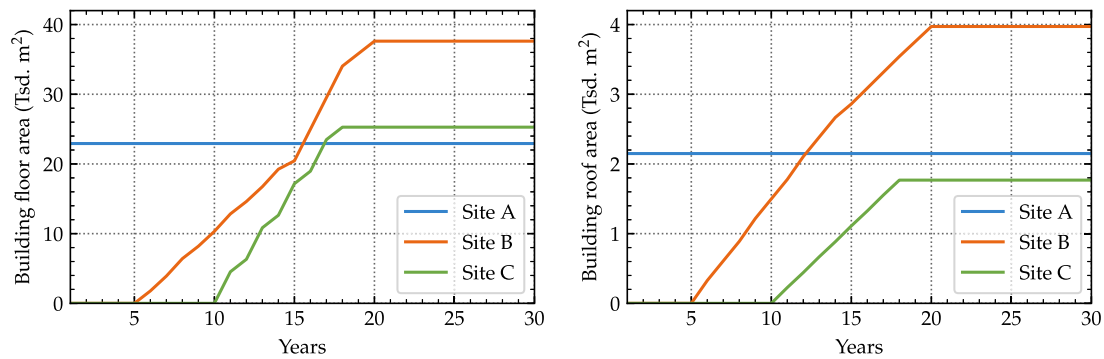
Fig. 4. Evolution of total building floor area (left) and total roof area for the installation of solar technologies (right) for the three sites of the case study urban development during the 30-year planning period.
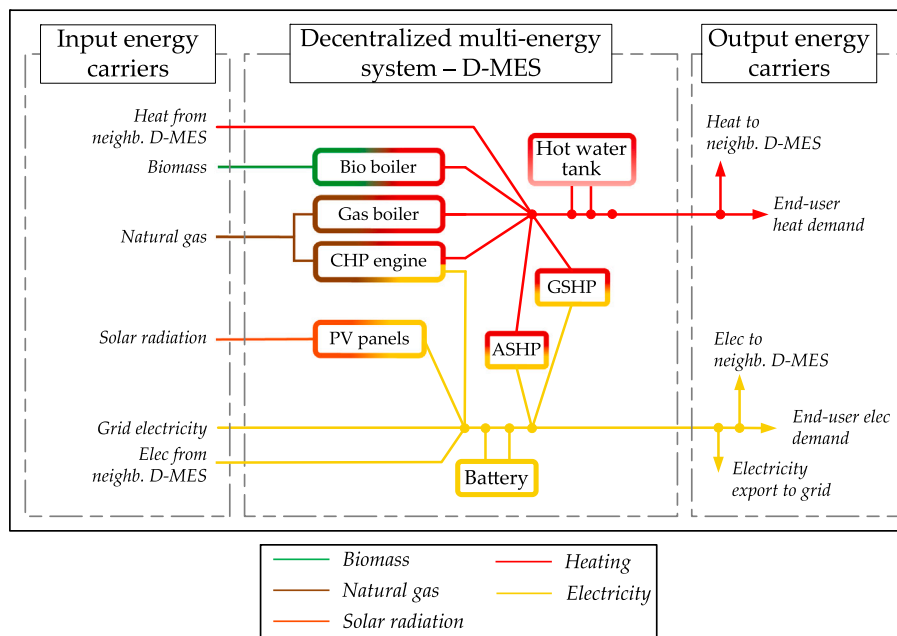

Fig. 5. Superstructure representation of candidate energy conversion and storage technologies for the composition of a D-MES.

of an energy system for a hypothetical urban district in the city of Zurich, Switzerland. A 30-year planning period is considered (2021–2050) and the urban development is composed of one existing (site A) and two new neighborhoods (site B & site C), which are assumed to be developed in different construction phases. These exemplary development phases are inspired from an actual D-MES district near Zurich [45,46]. A summary of the urban district's development plan is shown in Fig. 3 and is discussed as follows:

- Site A corresponds to an existing, mixed urban neighborhood composed of 4 single-family houses (SFH), 16 multi-family houses (MFH) and 4 commercial buildings. The exact configuration of this existing urban district in terms of building geometries, placement and characteristics is taken from [47]. The total building floor area for this site is approximately 22'300 m^2.
- Site B is a new development with construction taking place in two phases. In the first development phase (Phases 2 and 3), between 2026 and 2035, a total of 45 residential buildings (13 SFH and 32 MFH) are built with a total floor area of 20'450 m^2. In the second development phase (Phase 4), between 2036 and 2040, 1 commercial office building is constructed per year, for a total of 5 office buildings with total floor area equal to 17'200 m^2. Hence, the total building floor area for site B after both construction phases are complete will be approximately 37'650 m^2.

- Site C is a also a new district, however, it is assumed to be composed purely of commercial consumers with 1 commercial office buildings being built each year between 2031 and 2038 for a total building floor area of 25'300 m^2 when construction is complete.

The evolution of the total building floor and roof area that is suitable for solar installations over the 30-year planning horizon is shown for each site of the district in Fig. 4.

3.2. D-MES design task, scenarios and a sensitivity analysis

3.2.1. Design task description

The envisioned energy system for the case study urban district is composed of three D-MES, each of which will be installed at one respective site and will supply the site's buildings with thermal and electrical energy to cover their heat (space heating and hot water) and electricity (appliances, lighting and air-conditioning) demands. The technology portfolio that is considered for each site's D-MES are given in a superstructure representation in Fig. 5. In terms of conversion technologies, the candidate technologies include electrically-driven air-source heat pumps (ASHP), ground-source heat pumps (GSHP), natural gas and biomass boilers, and gas-fired combined heat and power (CHP) engines. In terms of renewable energy technologies, photovoltaic (PV)
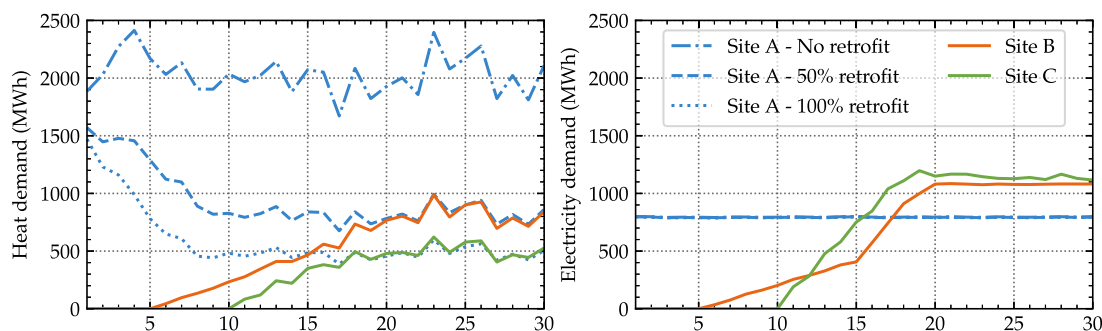
Fig. 6. Evolution of heat (left) and electricity (right) demands for the three sites and the three retrofit scenarios during the 30-year planning period.

panels are considered. Additionally, hot water thermal storage tanks and lithium-ion batteries are considered to store thermal and electrical energy, respectively. Each D-MES can import biomass from external sources and is connected to the natural gas and the electricity grid, allowing for imports of natural gas and imports and exports of electricity. Finally, the option for interconnecting the three D-MES is also included in the case study to consider the possibility of sharing resources and exchanging energy during low energy demand times at one site and high energy demand times at another. These energy exchange possibilities are also shown in Fig. 5.

Given the case study's development plan, in this paper, to demonstrate long-term, multi-stage energy planning for urban districts, we opt for a 6-stage investment plan with investment stages occurring every 5 years (*i.e.* in the beginning of 2021, 2026, 2031, 2036, 2041, and 2046, respectively).

Overall, then, from an energy system design perspective, the district's energy plan will prescribe *which technologies* need to be installed for *each site* at *each investment stage* and whether *interconnections* between the sites need to be built. Additionally, since the model also calculates the optimal energy system operation for the whole planning horizon, some insights with regards to the system's operation (*e.g.* the utilization of each technology at each site, imports, exports and exchange of energy) will also be provided.

3.2.2. Scenarios

For the D-MES design problem described in the previous section, the MANGO model is used to identify multiple optimal solutions to represent the trade-offs between the system's total cost, expressed in net present value terms for the year 2021, and the system's CO_2 emissions, calculated as the total over the project horizon. However, to gain further insights regarding some key model aspects and case study characteristics, we define and investigate a series of scenarios. The first of these aspects is the influence of D-MES interconnections on the system design and performance. As a result, we define two scenarios: with and without D-MES interconnections.

Given that, unlike sites B and C, site A is composed of existing buildings, a second aspect that we would like to examine is the influence that potential retrofits for site A's buildings would have on the energy system design results. Building retrofits that increase the thermal energy efficiency of the buildings in site A would alter the shares of thermal energy demands among sites and could in turn also alter the system's operating patterns and performance.[8] To examine this, we define three scenarios: one with no building retrofits, one in which 50% of the buildings are retrofitted, and a last one where 100% of the buildings are retrofitted. In the '50% retrofit' scenario buildings are ranked in terms of their energy demands and the twelve buildings

with the highest total heat demands are chosen to be retrofitted. For both the 50% and the 100% retrofit scenarios, buildings are to be fully retrofitted (addition of wall, roof, and ground floor insulation along with window replacements) with the retrofitting process occurring in the first 10 years of the project (2021–2030)[9].

The retrofit interventions affect primarily the building heat demands, by reducing the buildings' space heating demands, while the hot water demands remain unaffected. On the other hand, retrofitting has only a small influence on the site's electricity demands, by reducing the air-conditioning loads, while the electricity demands for lighting and appliances, which form also the largest electricity demand share, remain unaffected. Retrofit costs for each building are calculated using the information in [48] and are attributed to each year in accordance with the retrofit schedule. After the MANGO model calculates the total and yearly D-MES costs, the annual retrofit costs are added to them, to obtain the overall scenario cost.

In order to study the interactions between interconnection and retrofit options, all possible scenario combinations are considered, bringing the total scenario number to six.

3.2.3. Sensitivity analysis

In addition to the interconnection and retrofitting scenarios, we also perform a brief sensitivity analysis to understand the impact that investment flexibility, expressed as the number of investment stages considered, has on the resulting energy plan. We perform the sensitivity analysis for the cost-minimization objective under the scenario without D-MES interconnections and without retrofits. Under these settings, we then compare the multi-stage investment plans under 3, 6, 12, and 18 investment stages. A comparison with a single-stage plan is not performed, since the class of static, single-stage D-MES design models cannot be applied for multi-stage design problems.

3.3. Case study input data

The input data to the model that pertain to the case study can be divided into three key categories: (i) the energy demand patterns that each D-MES need to satisfy and the incoming solar radiation patterns on the building rooftops of each site, (ii) the investment costs and technical characteristics of all energy conversion, storage and distribution technologies considered, and (iii) the energy carrier prices and emission factors. The latter points (ii) and (iii) are presented in Tables B.6, B.7, B.8, B.9, and B.10, while the former point (i) is presented in Fig. 4.

---

[8] Electric energy efficiency interventions were not considered, as electricity demand levels for lighting and appliances were calculated considering state-of-the-art norms.

---

[9] We assume that for the '50% retrofit' scenario, two buildings are retrofitted in each of the first two years, followed by one building per year for the remaining eight. For the '100% retrofit' scenario, three buildings are retrofitted in each of the first four years, and then two buildings per year for the remaining six.
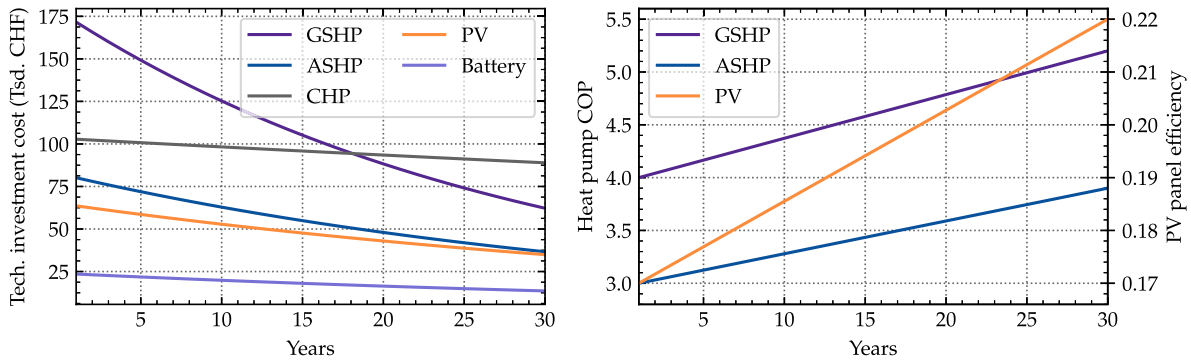
Fig. 7. Evolution of investment costs for a 100 kW-sized ASHP, GSHP, CHP and PV system and a 100 kWh-sized battery during the model horizon (left) - The total technology investment cost reflects the contributions by both the fixed cost (fc) and the linear cost (lc) terms, as given in Table A.3. Evolution of heat pump Coefficient-of-Performance (COP) and PV panel efficiency during the 30-year planning period (right).
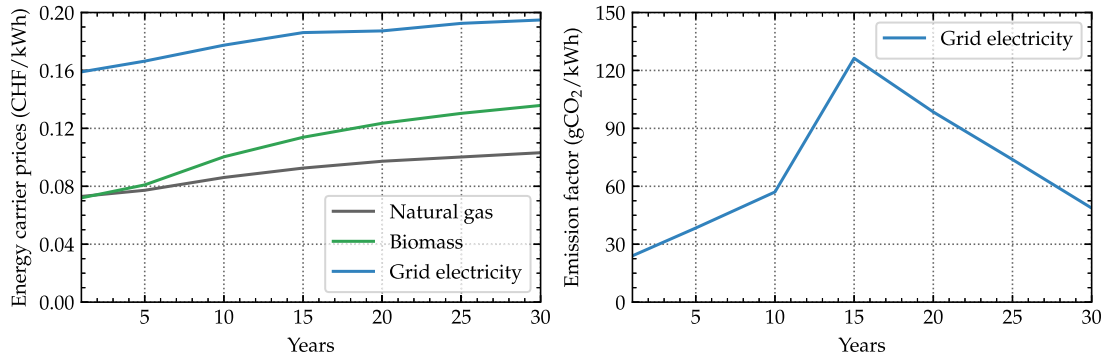

Fig. 8. Evolution of energy carrier prices (left) and grid electricity emission factor (right) during the 30-year planning period.

3.3.1. Site energy demands and renewable potential

The heat and electricity demands and the incoming rooftop solar radiation for each building in the district are calculated using the Building Performance Simulation software EnergyPlus [49]. To represent the inter-annual variability of weather conditions, as well as the changing climate conditions during the planning horizon, each building in its respective site is simulated for every individual year between 2021–2050, using weather files that were developed in [47] and describe future climate conditions for the case study's location.

The building geometries, locations and characteristics (building age and constructions) for site A are taken directly from [47]. For the retrofit scenarios, the buildings of site A are assumed to reach the retrofit construction standards set in the latest construction standards in Switzerland. The same set of building geometries as for site A are then also used to compose sites B and C, however, the building constructions are updated to reflect the latest construction standards in Switzerland [50]. By year 30, thermal demands for site A thermal energy demands are reduced by 60% and 75% in the '50' and the '100% retrofit' scenarios, respectively.

Fig. 6 shows the evolution of the annual heat and electricity demands for the three sites. In the 'No retrofit' scenario, site A's heat demand is dominant over the whole planning horizon. In both retrofit scenarios, site A's heat demands show a decreasing trend for the first ten years and reach similar levels as site B in the '50% retrofit' scenario and as site C in the '100% retrofit' scenario. On the other hand, as soon as their construction phases are complete, both sites B and C exhibit higher electricity demands compared to site A, primarily due to the large areas of commercial space.

The final processing step necessary for efficient optimization solver time is to convert the hourly energy demand and solar radiation profiles for each site and year into a set of typical days that can represent the full year. This is done in two steps: In the first step, similarly to many previous research efforts [21,51,52], the *k*-medoids clustering

algorithm is used to select the five most representative days of each year considering all sites' energy and solar profiles. In the second step, for each development phase (*i.e.* the years between two investment stages), the days when the peak heating and the peak electricity demands occur for each site are also added to their corresponding year. This second step, thus, ensures that between two investment stages, the peak demands for each site are considered and the design will ensure adequate system capacity to meet them.

3.3.2. Technology costs and technical characteristics

Given the multi-year horizon of the MANGO model, all technology costs and technical characteristics, along with best estimates regarding their evolution, need to be defined for every individual year and investment stage. For this case study, we have assumed that during the project planning horizon the technology costs and characteristics for less mature technologies, such as PV panels or batteries, will change driven by technological learning and efficiency improvements. For more mature technologies like natural gas boilers, on the other hand, constant values are taken for both the technology costs and performance characteristics like conversion efficiencies. An extensive data collection campaign was launched, comprised of both scientific publications and technical reports, to characterize the necessary data for the relevant parameters of all considered technologies until 2050. Actual values and data sources are presented in the Appendix B. As examples, Fig. 7 shows, first, the assumed technology cost evolution for a 100 kW-sized ASHP, GSHP, CHP and PV system and a 100 kWh-sized lithium-ion battery, which decrease at various learning rates from 2021 to 2050. The figure also shows the assumed improving efficiencies for heat pump technologies and PV panels.

3.3.3. Energy carrier prices and emission factors

To determine the evolution of energy carrier (natural gas, biomass, electricity) prices for the complete project horizon, current consumer
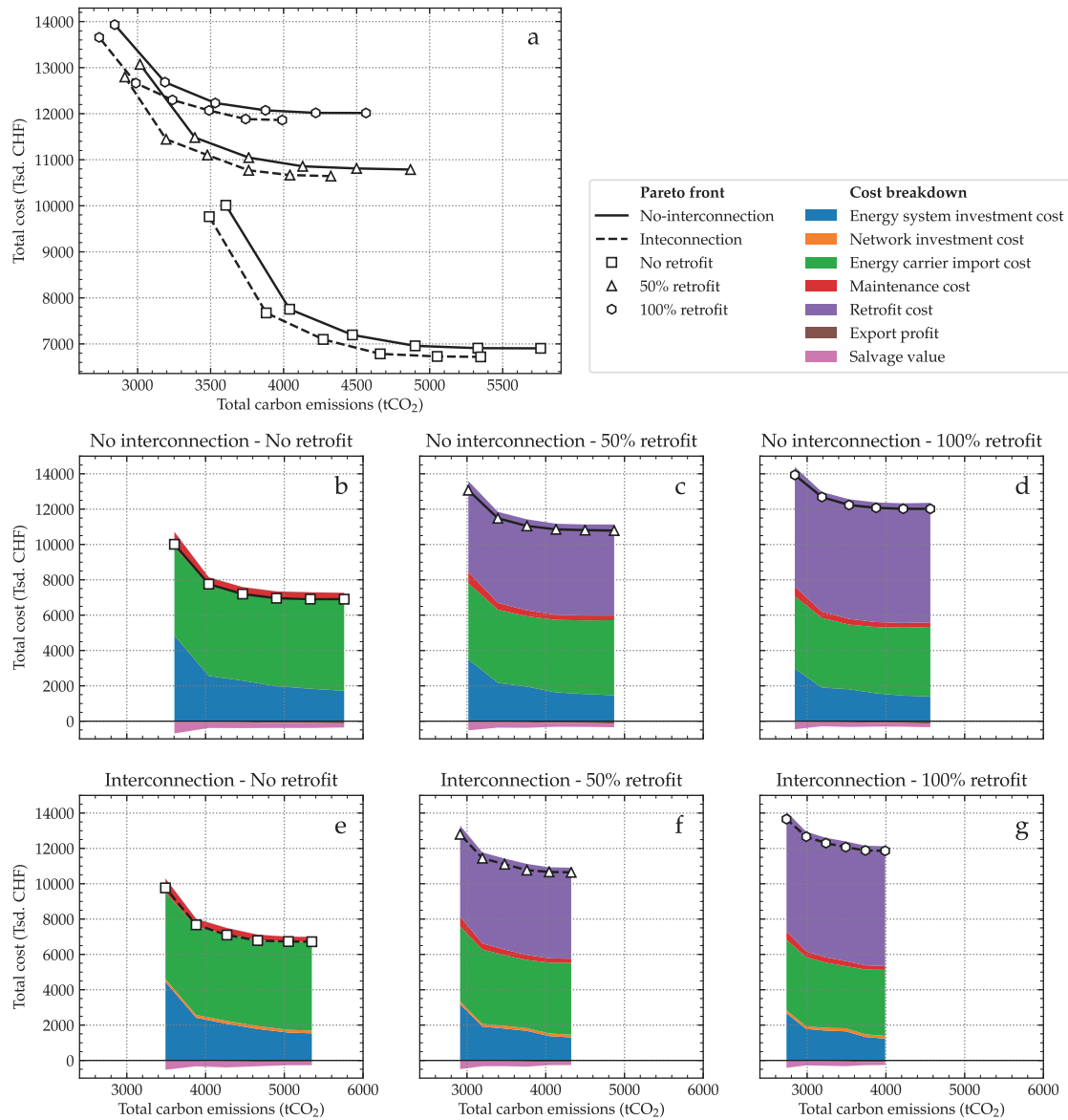
Fig. 9. (a) Pareto front illustrating the total system cost and CO$_2$ emissions for the optimal D-MES designs in the six interconnection–retrofit scenarios. (b-g) Breakdown of total system costs along the Pareto front for the six scenarios.

prices are taken from the Official Energy Statistics of Switzerland [53] and are assigned as prices for 2021. Then, the evolution of these prices is assumed to follow the New Energy Policy (NEP) scenario of the Swiss Energy Strategy 2050 [54], which limits emissions to 1–1.5 tCO$_2$ per person in 2050. The resulting price developments are given in Fig. 8, demonstrating a gradual increase for all considered energy carriers.

The carbon emission factor for natural gas is assumed constant and equal to 198 gCO$_2$/kWh for the whole planning horizon, taken from [54]. Since life cycle analysis of technologies is not considered in this work, neither biomass consumption, nor electricity generation from PV panels, are assumed to incur any CO$_2$ emissions. However, the carbon intensity of grid electricity imports to the district are expected to vary from year-to-year in the modeled horizon, driven by changes in the generation mix, which are in turn driven by market conditions, policy targets, etc. at national and international levels. To model the evolution of the Swiss grid's carbon intensity relevant for this D-MES, we first assign today's carbon intensity (24 gCO$_2$/kWh, taken from [55]) as the value for 2021. Then, we model its development according to the NEP scenario and the Variant C&E electricity supply scenario, as expressed in the Swiss National Strategy 2050 [54]. The evolution of the resulting

grid carbon intensity is also presented in Fig. 8. The shape of the curve is explained by the fact that the C&E scenario assumes that in the first 15 years (2021–2035), Swiss nuclear power plants[10] are replaced by equal shares of renewable and fossil fuel technologies (decentralized CHP and Combined Cycle Gas Turbine (CCGT) plants), leading to the increasing trend for the grid's carbon intensity. From year 15 onward, fossil fuel plants are gradually phased out, while renewable generation keeps increasing, leading to the subsequent decreasing trend.

4. Results

In this section, we present the main results of applying MANGO to the dynamic urban development case study, highlighting the main insights that multi-stage design results can offer to D-MES developers. First, the economic and environmental performance of the optimal D-MES designs in the different scenarios are presented in Section 4.1. Then the optimal system configurations are discussed in Section 4.2,

---

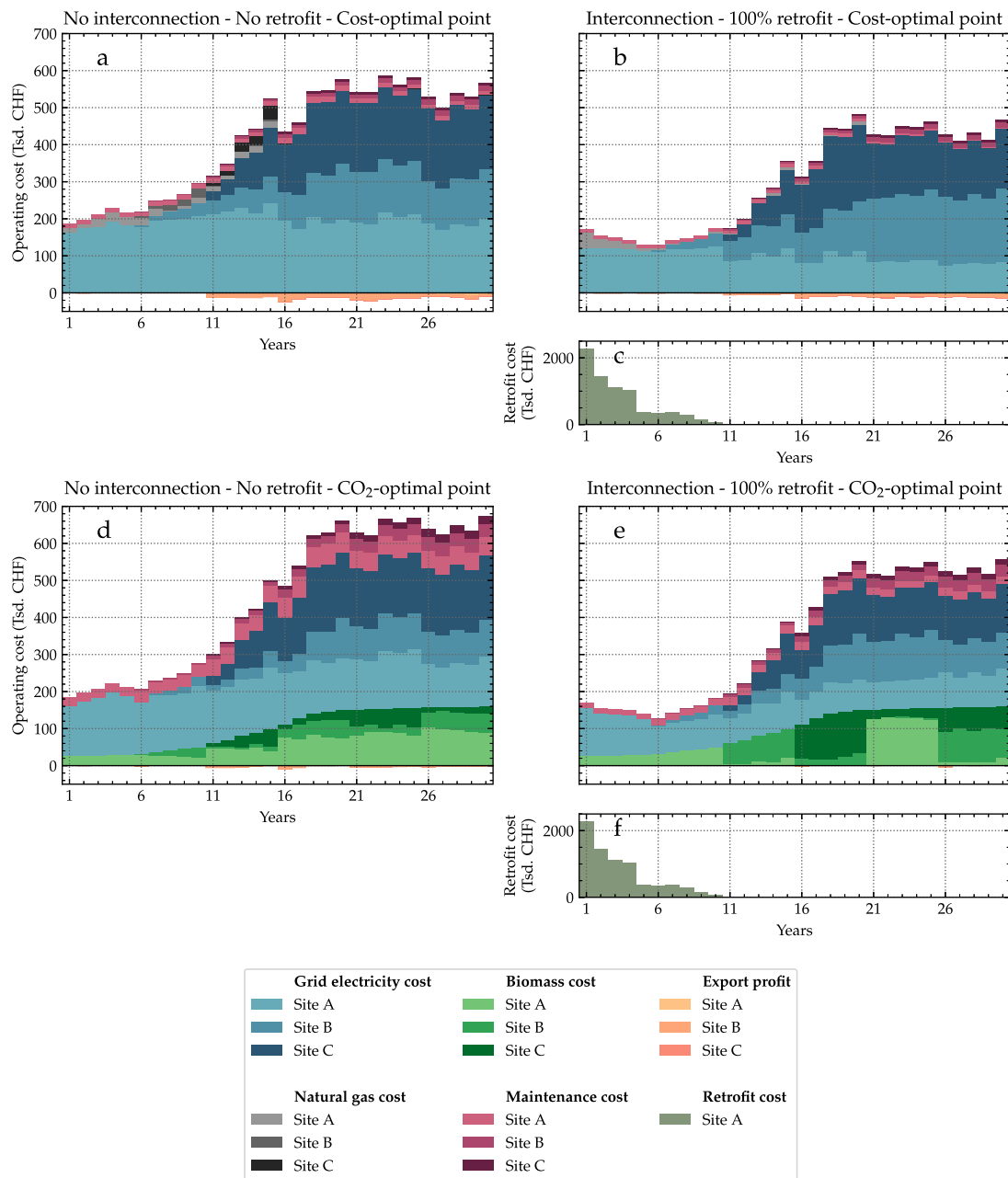[10] Switzerland has committed to phase out nuclear energy by 2034 [56].

Fig. 10. Operating (a-b, d-e) and retrofit costs (c, f) over the 30-year planning period for two interconnection–retrofit scenarios and for the cost- and CO$_2$ optimal Pareto points. The costs in this figure correspond to nominal, undiscounted expenditures.

alongside insights on their operating patterns in Section 4.3. The results of the sensitivity analysis are presented in Section 4.4, and, finally, a results and model discussion is provided in Section 4.5.

4.1. Economic and environmental performance of optimal D-MES design

Fig. 9a presents optimal Pareto fronts for all retrofit and interconnection scenarios that illustrate the direct trade-offs between D-MES costs and CO$_2$ emissions. Overall, in all cases, starting from the cost-optimal point, emission reductions can be achieved with small increases in the total system cost. For instance, for an emission reduction of approximately 20%, costs increase 2–5.5% in all scenarios. However, CO$_2$-optimal points lead to sharp cost increases that are 15% higher than the cost-optimal points in the case of the '100% retrofit' scenarios and even 45% higher in the 'No retrofit' scenarios.

Observing the scenarios more closely, we observe major differences in their resulting economic and environmental performance. Under all retrofit scenarios, allowing D-MES interconnections shifts the Pareto fronts towards both lower costs and lower emissions. Comparing, for instance, the results of all cost-optimal points, interconnections lead, on average, to 10% less emissions and 2% lower costs.

On the other hand, retrofitting allows for substantial emissions reductions, but also leads to higher costs. For instance, the emissions of the CO$_2$-optimal points of the '100% retrofit' scenarios are lower by more than 20% compared to the corresponding points in the 'No retrofit' scenarios. However, the costs in the cost-optimal points of the '100% retrofit' scenarios are on average 75% higher than the cost-optimal points without retrofitting. As a result, depending on the CO$_2$ levels that the developer wants to reach or that are mandated by energy regulations, retrofitting might be an important element of the energy plan for the case study district. It should be noted, though, that, in this
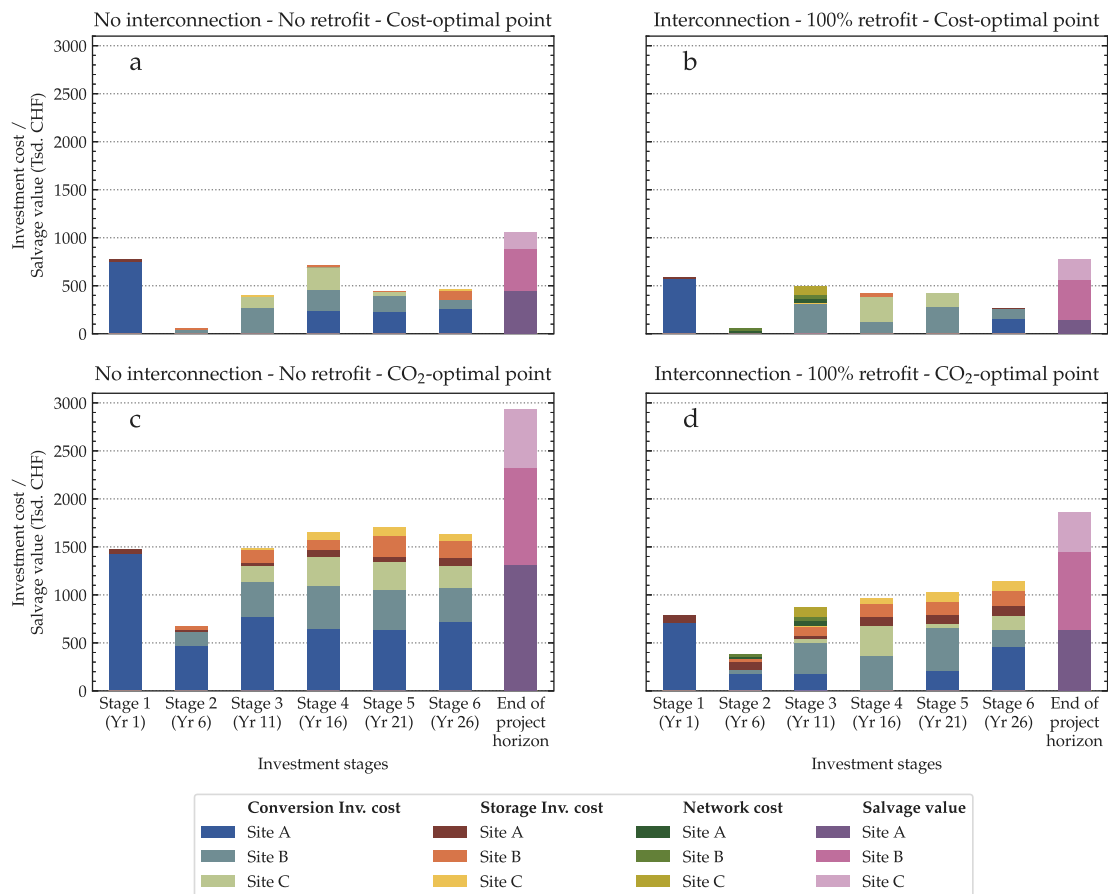
Fig. 11. Total investment costs per investment stage for two interconnection–retrofit scenarios and for the cost- and CO_2 optimal Pareto points. The costs in this figure correspond to nominal, undiscounted expenditures.

work, we only represent the retrofit-related costs, but not the potential economic benefits due to higher building value after the retrofits. If these were to be included, the retrofit-related cost increases could be reduced.

The influence of interconnections and retrofitting on the system cost and emissions is further illustrated in Fig. 9b-g, which show the breakdown of costs across all Pareto points and scenarios. Across the same interconnection scenarios, retrofitting leads to reductions of the D-MES-related costs, which are, however, offset and exceeded by the retrofit costs themselves, leading to overall increased costs. Under the same retrofit scenario, however, allowing D-MES interconnections adds a comparatively low cost for the network technologies, but, by reducing primarily the investment costs, leads to overall lower system costs and CO_2 emissions. Finally, across all cases, the energy carrier import costs are the most dominant D-MES cost category, responsible for 50% to 75% of the total system cost (excl. retrofit cost) across all cases, followed by the energy technology investment costs, which correspond to 23% to 48% of the total system cost (excl. retrofit cost). Maintenance costs, network investment costs and revenue sources have a minor influence on the overall cost.

Besides the overall economic and environmental performance of the studied systems, MANGO, with its multi-year perspective, also provides information regarding the evolution of the system costs. For a few selected scenarios, Fig. 10 presents the evolution of the operating costs and revenues for the D-MES of all sites and the yearly retrofit costs for site A. The corresponding plot regarding the evolution of the CO_2 emissions for the D-MES is given in Fig. C.17. Please note that all future costs and revenues in the figure are not discounted to demonstrate their relative magnitude. The overall trend shows a clear increase in future operating costs, driven partly by the developments in sites B and C (see

Fig. 3), and partly by the projected increases in energy carrier prices (see Fig. 8). On the other hand, the retrofit cost evolution shows a decreasing trend, since the bigger buildings with higher energy demand levels are prioritized in the retrofit plan, as discussed in Section 3.2.2.

Taking a closer look at the individual cost categories, while retrofitting reduces system operating costs, the allocation of import costs across the energy carriers remains the same between the two cost-optimal points and the two CO_2-optimal points in Fig. 10. For example, for the cost-optimal cases, the grid electricity cost is the dominant operating expenditure, exceeding 90% of the total operating cost in some years, but it also remains important for the CO_2-optimal points too, with biomass cost showing also increased influence. Furthermore, in CO_2-optimal points, there is a noticeable reduction in export profit due to higher self-consumption of locally generated PV electricity in order to reduce system emissions, along with a growing influence of maintenance costs, as a consequence of higher overall technology investment costs[11] for these points shown in Fig. 9. Finally, although we do not present the isolated impact of interconnection in the figure, results showed that it does not greatly influence operational costs but instead the cost composition between sites, since in this case one site can increase energy production to cover the energy demands on different sites.

Next, the results for the evolution of the technology investment costs are presented in Fig. 11. The same scenarios as the ones of Fig. 10 are also used here and the costs reported are the nominal, undiscounted values. Starting from the impact of retrofits and interconnections on

---

[11] Maintenance costs for a technology are calculated as a percentage of the upfront investment cost for the technology, as shown in Eq. (A.10).
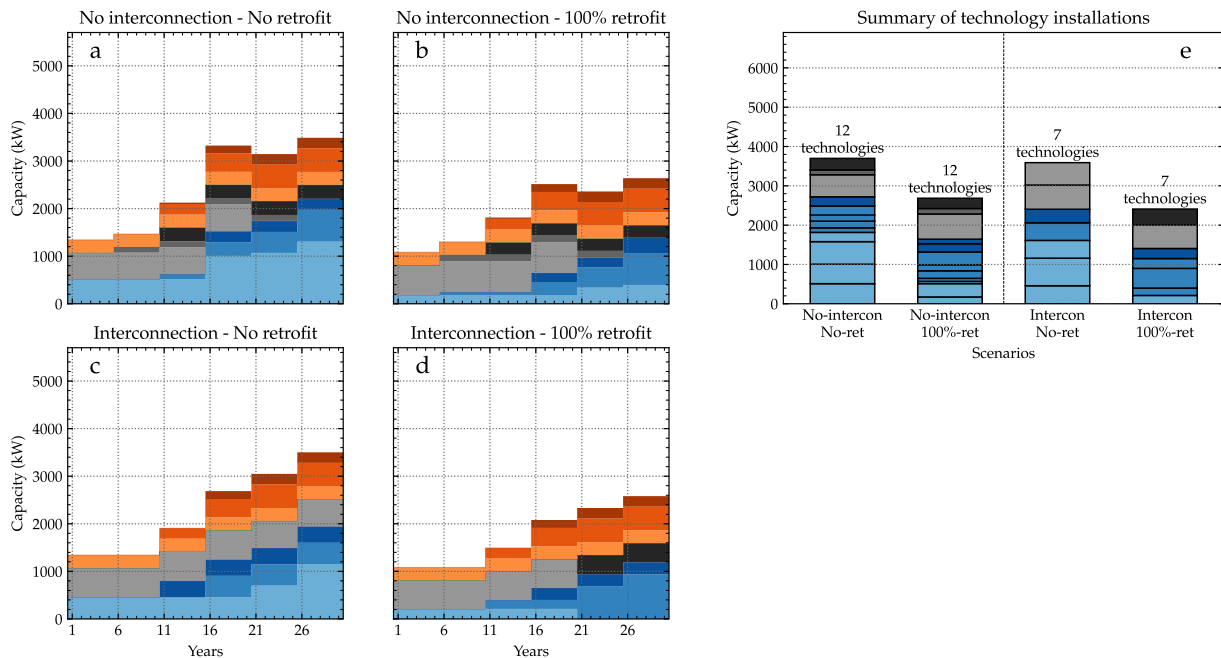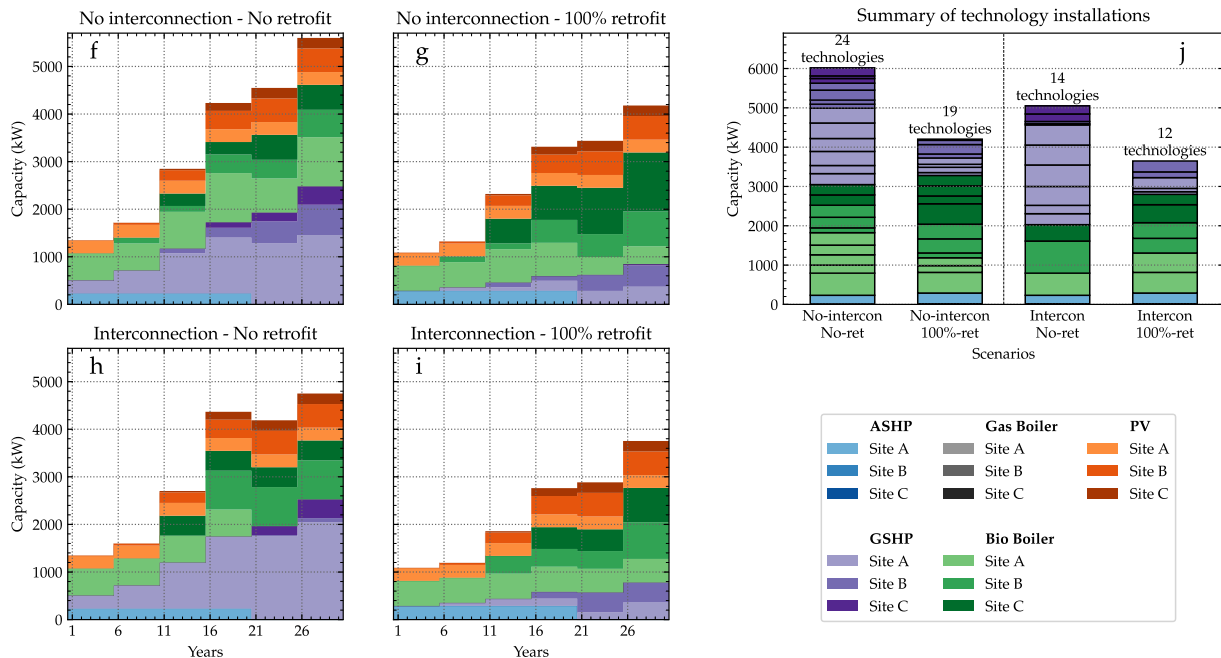
Fig. 12. (a-d, f-i) Evolution of installed capacities of energy conversion technologies at each site during the 30-year planning period for four interconnection–retrofit scenarios and the cost-optimal (a-d) and CO_2-optimal Pareto points. (e,j) Summary of total, aggregated installed capacities of conversion technologies for four interconnection–retrofit scenarios and the cost-optimal (e) and CO_2-optimal (j) Pareto points.

investment costs, two key results are highlighted. First, for both the cost- and CO_2 optimal points, a reduction in the investment costs is observed, that is more pronounced in the CO_2 optimal case. Second, allowing D-MES interconnections incurs a change the investment patterns with fewer investments required per site and investment stage. For instance, in the case of the cost-optimal points with no interconnections, site A invests in conversion technologies in four stages, while when

interconnections are allowed, the number of investments is reduced to two.

Changing the axis of analysis and comparing the results under the same retrofit and interconnection scenario, Fig. 11 shows a significant increase in investment costs, when transitioning from the cost-optimal to the CO_2-optimal designs, which is equal to 200% in the 'No-retrofit' scenario and 125% in the '100% retrofit' case. Moreover, this increase is driven primarily by higher investments in conversion technologies and
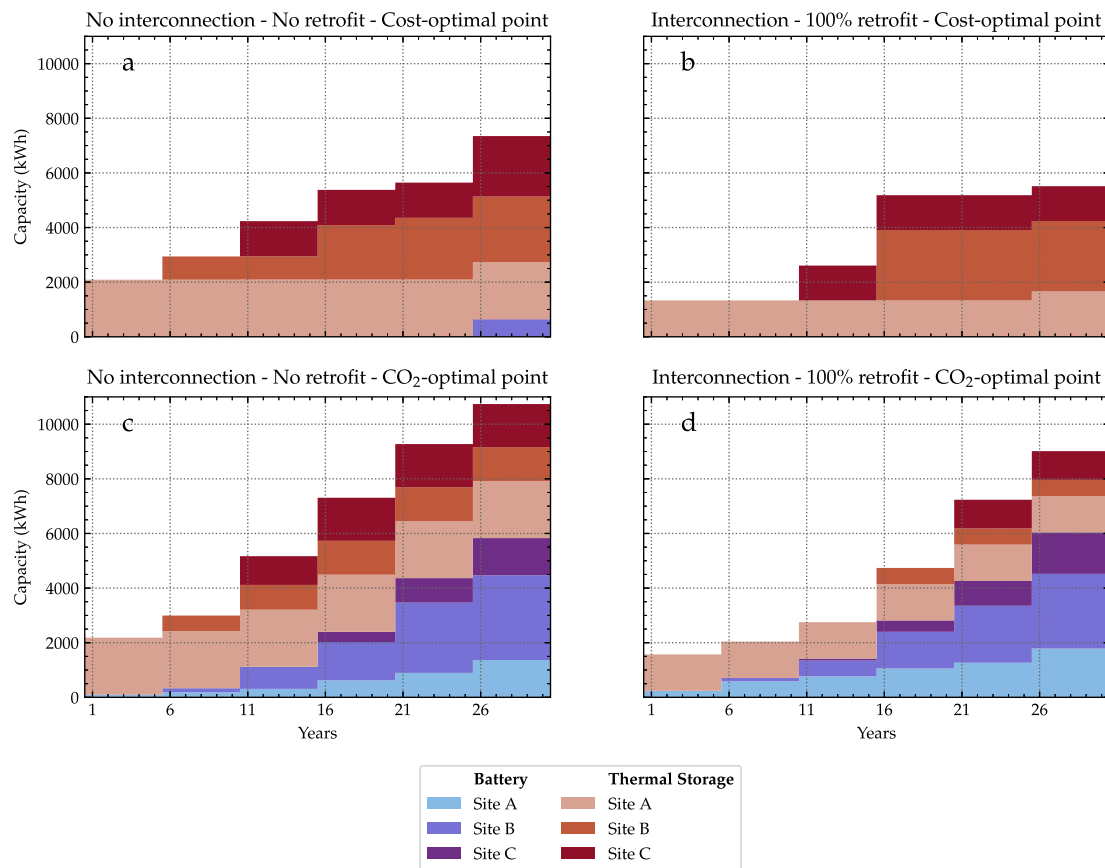
Fig. 13. Evolution of installed capacities of energy storage technologies at each site during the 30-year planning period for two interconnection–retrofit scenarios and the cost-optimal (a-b) and CO$_2$-optimal (c-d) Pareto points.

secondly in storage technologies. It is worth noting that, although not explicitly reported in Fig. 11, MANGO is capable of further breaking down investment expenditure per technology and site in order to provide more detailed information for the developer. Network costs in the interconnection scenarios have only a small impact. Finally, while the undiscounted salvage values appear to be very high due to the high investments towards the second half of the project horizon, actually the influence over the project time horizon is low, as observed in Fig. 9.

Overall, the results reveal complex investment patterns involving multiple investment options in each scenario and indicating that there is no dominant investment strategy among all cases. Hence, these results also highlight the value of multi-stage D-MES design tools that can deliver tailor-made and optimal plans that would not be easily discoverable with conventional planning approaches.

4.2. Technology configurations of optimal D-MES design

Following the system's economic and environmental performance, in this section, the technology configurations of the optimal D-MES designs are presented.

Fig. 12a-d and f-i offer valuable information pertaining to the evolution of the installed conversion technology capacities at each site, in four scenarios, and for the cost- and CO$_2$-optimal Pareto points. The scenarios represent the four possible combinations between the two interconnection scenarios and the 'No retrofit' and '100% retrofit' scenarios. It must be noted that to aid the readability of these figures, the available capacities of the same technology type in each year are aggregated before plotting. An example figure for one scenario with each individual installed technology shown separately depending on the investment stage in which it was installed is given in Fig. C.18.

Each individual technology installation is also considered in Fig. 12j with the bars stacking the capacity of each installation to present the sum of the installed conversion technology capacity over all stages for the four considered scenarios and for the cost- and CO$_2$ optimal points, respectively. For these two subplots, though, PV installations are excluded, since the total installed capacity is always maximized and equal across all scenarios.

Starting from the cost-optimal points in Fig. 12a-d, across all cases, the systems rely on ASHPs and natural gas boilers for the provision of heating. In the first years, natural gas boilers occupy the largest share of installed thermal capacity, however, the share of ASHPs in the total capacity increases with time, driven by the technology cost reductions and efficiency improvements shown in Fig. 7. PV installations are identical in all cases and their installation is maximized according to the available roof space during the case study development (see Fig. 4).

The overall impact of retrofitting and interconnection scenarios in the four studied scenarios is summarized in Fig. 12e. The main effect of retrofitting is the reduction in the total installed technology capacity for the systems, which is equal to −28% and −33% when interconnections are not and are considered, respectively. Under both interconnection scenarios, the reduction in installed capacity is mostly reflected on the ASHPs, while the natural gas boiler capacity remains relatively unaffected.

On the other hand, interconnections have only a small influence in the total installed capacity. However, in both retrofit scenarios, interconnections both (i) reduce technological complexity of the energy system and (ii) smooth capacity investments. Reduced technological complexity is demonstrated by the smaller number of larger thermal energy generation technology installations, such as ASHPs, reducing the total number of installed technologies, in both cases, from 12 to 7. The
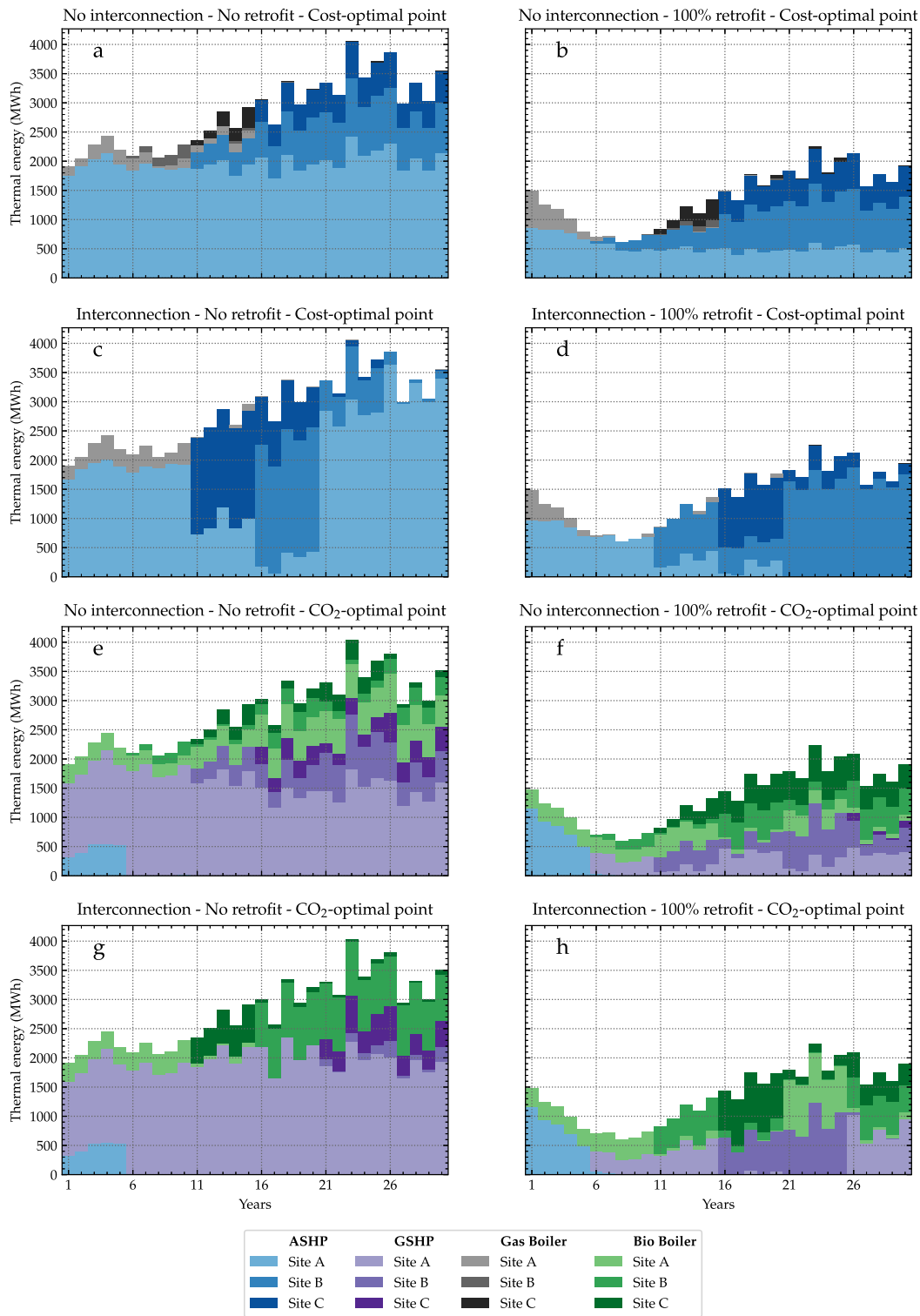
Fig. 14. Evolution of local thermal generation at each site during the 30-year planning period for four interconnection–retrofit scenarios and the cost-optimal (a-d) and CO_2-optimal (e-h) Pareto points.

influence of smoothing capacity investments are shown in year 16 of the interconnected cases due to ability to exchange thermal energy.

Shifting to the CO_2 optimal points, the first observation pertains to changes to the technology mix from gas boilers and ASHPs to a combination of biomass boilers and GSHPs. Additionally, there is a shift to larger technology capacities, driven by the greater reliance on GSHPs to self-consume locally generated renewable electricity and the addition of biomass boilers for a zero-carbon energy supply. The overall influence of retrofitting is the significant reduction in the total installed capacity (equal to −30% and −28% when interconnections are not and are considered, respectively), which is, in turn, translated to lower total GSHP and higher total biomass boiler capacities. Relating to the influence of interconnection, technological complexity is reduced in similar proportions relative to the cost optimal cases, for example from 24 to 14 in the 'No retrofit' scenario. In contrast to the cost-optimal case, though, interconnections also reduce the total installed capacity
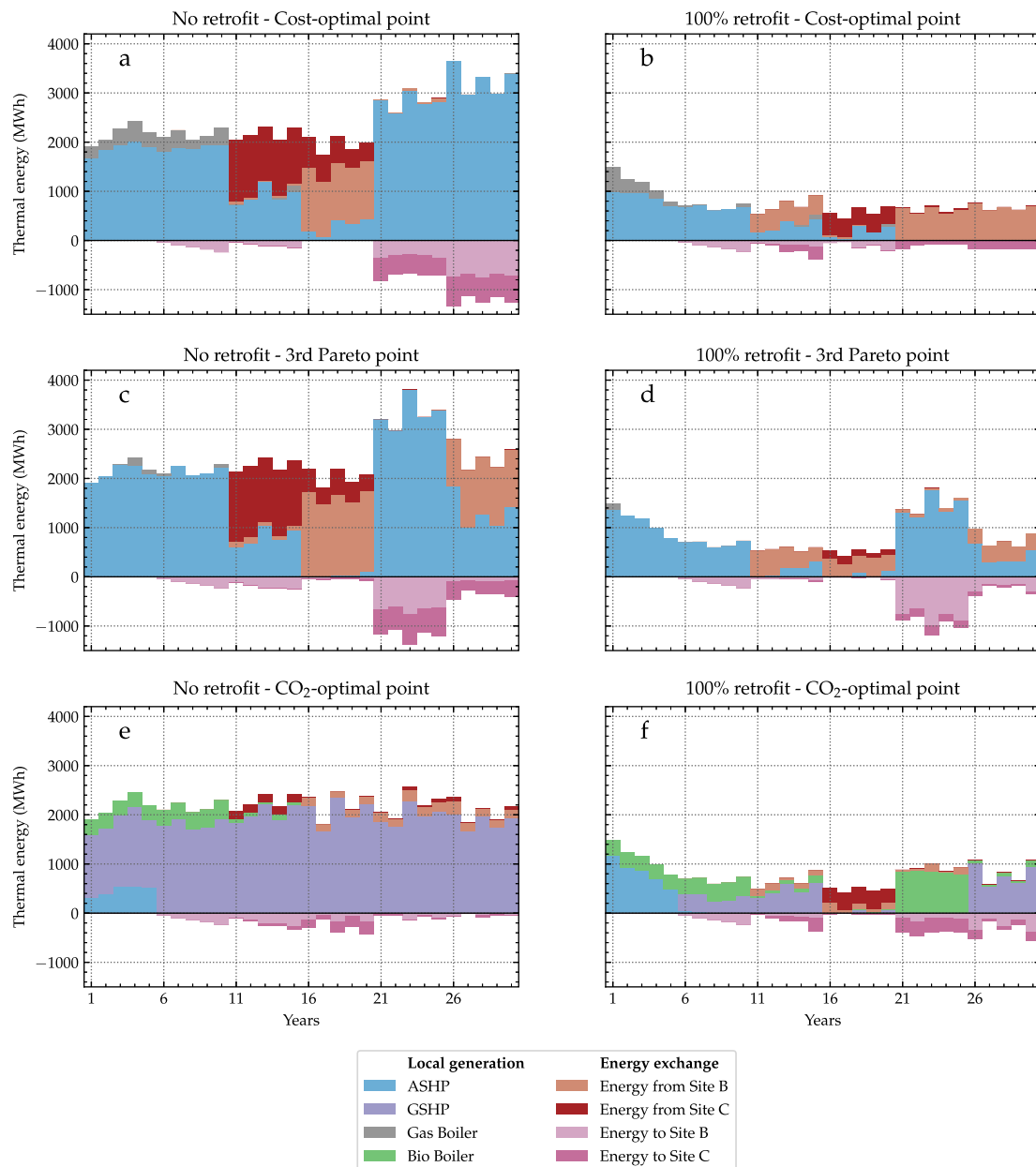
Fig. 15. Evolution of local thermal generation and energy exchange at site A during the 30-year planning period for the 'Interconnection' and the 'No retrofit' and '100% retrofit' scenarios and for the cost-optimal Pareto point (a-b), the 3rd Pareto point (with the 1st being the cost-optimal one) (c-d) and the CO_2-optimal (e-f) Pareto points.

for the CO_2-optimal points. However, the investment smoothing pattern observed in the cost-optimal results is not repeated here.

Shifting to energy storage, Fig. 13 presents the evolution of installed capacities for thermal storage and battery technologies at each site, in two scenarios, and for the cost- and CO_2-optimal results. Overall, similar patterns to Fig. 12 are observed, with total storage capacities growing over time across all cases. Retrofitting and interconnections reduce total installed capacities for the same Pareto points. Under the same scenarios, thermal storage plays a ubiquitous role, while batteries only become a major part of the energy system in the CO_2-optimal case.

4.3. Operating patterns of D-MES designs

Various streams of valuable information pertaining to the operation of the designed energy system are also provided by MANGO. One example is shown in Fig. 14, which presents the annual, total thermal energy generation per site over the time horizon for the same four

scenarios as in Fig. 12 and for the cost- and CO_2-optimal Pareto points (additional results on the evolution of local electricity generation and grid electricity imports is shown in Fig. C.19). Starting at the cost-optimal point and the 'No interconnection - No retrofit' scenario, we observe that natural gas boilers only produce a small fraction of the total thermal energy generation (11% on average per year) and are 'phased-out' after year 16. Thus, while gas boilers demonstrated similar capacities to ASHPs as shown in Fig. 12, they are operated as peak thermal energy supply. An overall similar pattern is observed for the 'No interconnection - 100% retrofit' scenario, with the only difference being that the ASHPs at site A produce less thermal energy due to retrofitting. The thermal generation patterns change drastically, though, as soon as interconnection is allowed. The key difference is that starting from year 10 onward, the largest share of thermal energy is primarily generated by technologies in one or two sites at a time, with energy demands at the rest of the sites met via the interconnections. This allows the overall system to better utilize newer technologies that have higher
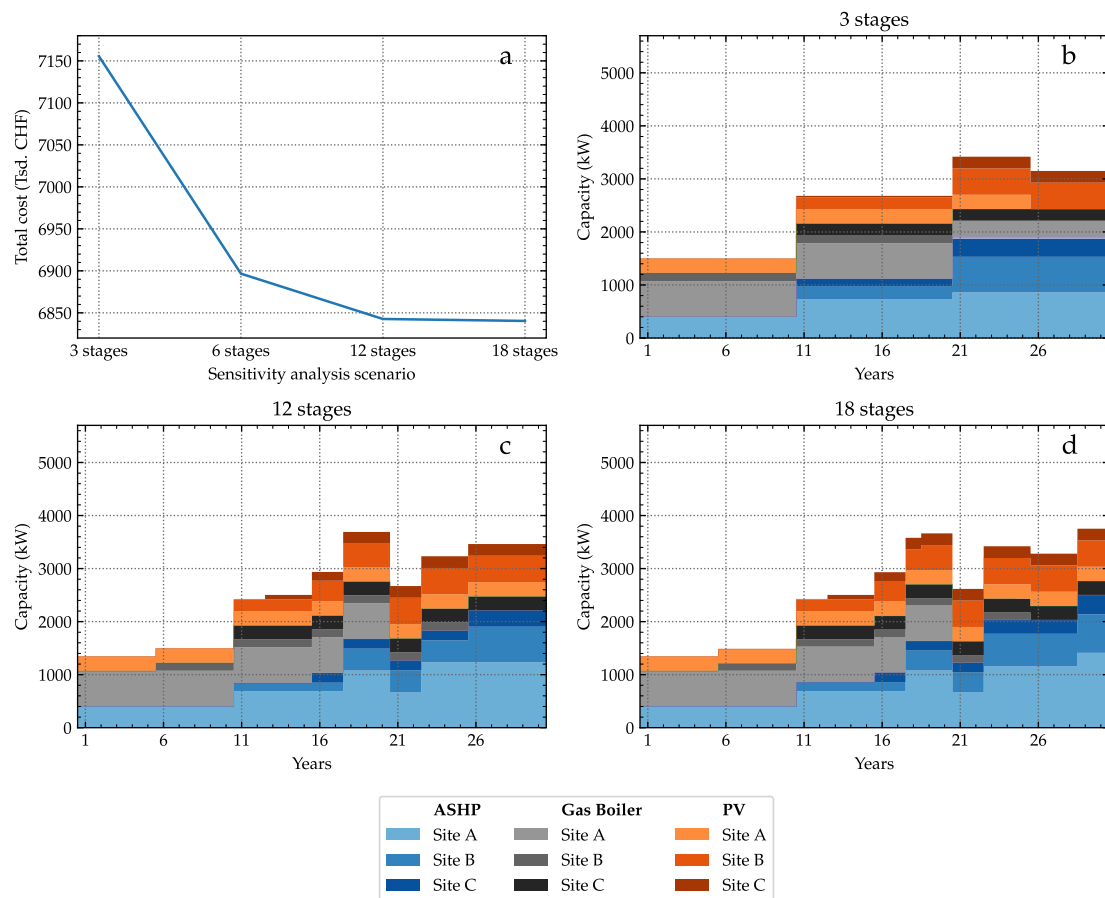
Fig. 16. (a) Total system cost for the 4 sensitivity analysis cases considered. (b-d) Evolution of installed capacities of conversion technologies at each site during the 30-year planning period in the sensitivity analysis cases with 3 (b), 12 (c), and 18 (d) investment stages. The corresponding results for the 6 investment stages are given in Fig. 12a.

efficiencies and have not experienced longer degradation times like older technologies. As an example, in the 'No retrofit' scenario, the new ASHP installed in year 10 at site B, generates more than 50% of the total thermal energy, reducing the share of site A's thermal generation. From year 21, as soon as a new ASHP is installed at site A, it becomes again the highest thermal energy generator. Similar patterns are generally observed in the '100% retrofit' scenario, however, due to site A's reduced heat demands, site B becomes the highest thermal energy generator, due to it also being the highest thermal energy consumer.

Comparing generally the scenario-by-scenario results between the cost- and CO_2-optimal points, we observe similar patterns for thermal energy generation. In the 'No retrofit' cases, the greatest share of thermal energy comes from GSHPs, exceeding 85% in some years, while biomass consumption is limited by the biomass availability constraints. Due to the lower heat demands for site A in the '100% retrofit' scenarios, biomass becomes the dominant heating technology. Similar to the cost-optimal cases, interconnection changes the shares of thermal energy generation between sites. While in the 'No retrofit' scenarios site A generates most thermal energy with GSHPs complemented by site B's biomass boilers, in the '100% retrofit case', the thermal energy generation patterns change between phases depending on which site has the newest and/or most efficient generation technologies. For instance, between years 16 and 20, sites B and C dominate with GSHPs and biomass boiler-based generation, while between years 21 and 25, the new and hence more efficient (due to less degradation) biomass boiler in site A takes over the biomass-based thermal energy generation from site B's D-MES.

Finally, Fig. 15 zooms in on one site and presents the local thermal energy generation and the thermal energy exchange from the perspective of site A over the time horizon, for the cost-optimal, the 3rd

Pareto point (see Fig. 9), and the CO_2 optimal solutions, in both the 'No retrofit' and the '100% retrofit' scenarios. Starting from the 'No retrofit' results, site A, in the cost-optimal and 3rd Pareto point cases, initially covers its own thermal energy demands until year 10, then relies primarily on energy imports from other sites until year 20, and then transitions back to covering its own thermal energy demands and exporting to other sites. Overall, in these two cases, site A covers 80% and 68% of its thermal needs through local generation and the rest through imports. On the other hand, for the CO_2-optimal point, site A becomes highly self-sufficient covering 94% of its energy demand through local generation, primarily using GSHP technologies, leading to very low amounts of energy are exchanged from and to site A.

Retrofitting does not change the thermal energy landscape for site A, which still relies on combinations of local energy generation and energy exchange at different shares during the model horizon, albeit at lower levels due to the lower heat demands. However, in the case of the CO_2 optimal solution, much more complex patterns emerge with periods in which combinations of technologies are used to generate heat locally and exchange it to other sites, and periods *e.g.* between year 16 and 21, during which energy exchanged from other sites is used to cover heat demands. In total, over the project horizon, site A covers 52%, 75% and 86% of its own thermal requirements in the cost-optimal, 3rd Pareto point, and CO_2-optimal solutions, respectively.

4.4. Sensitivity analysis

Fig. 16 summarizes the main results of the sensitivity analysis described in Section 3.2.3. Starting from the system's economic performance, Fig. 16a compares the total system cost resulting from cost-optimal plans with 3, 6, 12 and 18 investment stages. Results show

a decreasing cost trend as the number of investment stages increase. While the 3-stage plan has approximately 4% higher costs than the base case, 6-stage plan, increasing the number of stages to 12, and further 18, incurs a decreasing marginal benefit. This indicates that the additional planning flexibility above 12 stages cannot be harnessed in this specific case study, but nonetheless demonstrates the value of multi-stage modeling approaches.

Fig. 16b-d further present the evolution of the energy system's composition for 3, 12 and 18 investment stages, which can be contrasted with the base case, 6-stage plan from Fig. 12a. Overall, the same general trends can be observed in all cases with a split between natural gas boilers and ASHPs in the first years and a transition to higher ASHP capacities towards the end of the model horizon. Additionally, PV capacities are always also maximized. Nevertheless, as the number of investment stages increases, also the complexity of the resulting plan increases too. This can be observed especially in the 12- and 18-stage plans, with a larger number of smaller capacity additions happening after year 16. Overall, a trade-off is formed between system cost and technological complexity. Depending on the priorities of the developer, an appropriate number of investment stages can be selected.

Finally, although we have not performed formal tests, a brief note is provided regarding the computational time required for the different cases, which, as discussed in Section 2.3, increases with the number of stages considered. In our simple sensitivity analysis, the computational time varied exponentially from approximately 10 min when 3-stages are used, to approximately 1 h with 6 stages and more than 2 days when 18 stages are used. These are only provided as an indication here and can vary significantly depending on the details of the scenario considered (*e.g.* with or without interconnections etc.).

4.5. Results and model discussion

In this section, we provide our perspective on the added value that MANGO's D-MES design approach can bring for energy developers and, finally, we provide a brief discussion on the important issue of uncertainty.

As discussed in the Introduction, the process of creating D-MES planning strategies for an urban district should reflect its dynamic construction development, as well as the long-term developments of the surrounding energy and economic landscape. MANGO incorporates the most relevant dynamic aspects for D-MES, such as evolving energy prices, technological developments, and changing energy demands due to retrofitting and/or new building additions, and is capable of generating optimal D-MES planning strategies with the desired flexibility in terms of the number and frequency of investment stages.

The incorporation of a multi-year horizon, along with multi-location D-MES configurations, each of which is composed of multiple technologies, means, on the one hand, that MANGO is capable of delivering highly complex plans. Overall, MANGO offers a wealth of information, across different dimensions that can be used to assist decisions at different strategic, economic, and technical levels. For instance, information on the total lifetime economic and environmental performance, as presented in Fig. 9, can be used at the strategic level regarding which of the proposed designs to choose. Detailed information regarding the yearly evolution of operation and investment costs, respectively in Figs. 10 and 11, can be used for project budgeting. The evolution of the installed technology capacities, as in Figs. 12 and 13, can be used at the technical level to guide purchasing decisions, while information on the year-to-year energy generation and exchanges, as presented in Figs. 14 and 15, can be used at the detailed engineering level when, for instance, deciding on the necessary infrastructure to coordinate multi-location D-MES operation. Finally, due to the multiple dimensions included in MANGO, all model outputs can be examined in close detail or abstracted in metrics defined per location and/or year for a more high-level view.

Besides the methodological contributions introduced by the proposed model of this paper, we aim to narrow the distance between D-MES modeling and real-world D-MES design in practical applications. We argue that the multi-stage investment perspective of the MANGO model matches more closely the needs of energy system developers when they design D-MES. Therefore, by highlighting the benefits of multi-stage D-MES design and the valuable insights that it can generate, we seek to contribute towards a faster diffusion of D-MES design optimization models from research to practice.

Despite its deterministic formulation, MANGO can nevertheless be valuable for real-world D-MES projects and practical applications. Although the model outputs a multi-year design plan, we do not expect D-MES developers to only run the model once at the beginning of a project and then fix all investment decisions for the project's duration. Instead, a developer should run the model with their best possible estimates of the model's dynamic parameters, obtain a multi-stage design plan for the D-MES that takes into account these developments, and then proceed to implement only the investments dictated by the model for the first investment stage with the knowledge of future flexibility. Then before the next, actual investment stage of the project, the developer should re-run the model, with updated estimates for the model's dynamic parameters and obtain an optimal decision for the next investment stage. Given that uncertainty grows larger the further the prediction horizon lies, one can have more confidence in their short-term predictions and, hence, the short-term investment decisions of the model that need to be implemented first.

5. Conclusions

This paper presented MANGO, a novel optimization model for the optimal, multi-stage design of D-MES. The model allows for flexible investment strategies to be defined and considers the most relevant dynamic aspects that evolve during the lifetime of a D-MES project, such as year-to-year variations in energy demands, changing energy carrier and technology prices, technical improvements in generation technologies and equipment degradation. MANGO further extends the state-of-the-art in multi-stage D-MES design, by allowing multi-location D-MES configurations to be optimized and by treating end-of-horizon effects for more accurate design decisions. Another novelty is MANGO's technology-focused modeling approach, which means that all investments in energy generation and storage are tracked separately and their capacities are not aggregated into total capacities. This allows the model to dispatch each installed technology individually taking into account their different performance characteristics *e.g.* due to performance degradation or due to technological improvements during the project lifetime.

In this paper, the MANGO model was also applied to a 6-stage D-MES design problem for an urban district case study in Zurich, Switzerland with the aim to demonstrate its application and highlight the insights that the model can generate. Total system cost and CO_2 emissions minimization are examined and six scenarios are also considered regarding D-MES interconnections and building retrofits.

Overall, the D-MES design plan in all optimization settings and scenarios benefit from the multi-stage investment strategy, as technologies are installed in all stages to echo the developments in the urban district, benefit from reduced future technology costs, and to replace technologies that reach the end of their lifetime. Regarding specifically the examined scenarios, results showed that allowing D-MES interconnections leads to better economic and environmental performance (for instance, 2% lower costs and 10% lower emissions on average for the cost-optimal designs across all scenarios). On the other hand, while retrofitting increases total costs significantly, it allows for lower CO_2 emission levels to be reached. For instance, the lowest possible emission level for the system without building retrofits is approx. equal to 3500 tCO_2. Under the '100% retrofit scenario', the minimum achievable emissions are reduced to approx. 2700 tCO_2. Regarding

technology configurations for D-MES, retrofitting and interconnections do not have a significant impact in terms of system selection, with most cost-effective designs including combinations of natural gas boilers, ASHPs and PV panels, while designs with the lowest CO_2 emissions transition to biomass boilers, GSHPs and PV configurations. Nevertheless, retrofits affect the total capacities of the technologies installed, while interconnections allow for technology sharing, and reduce the number of technologies installed. Finally, regarding the system's operation, interconnections allow for higher utilization of the newest, more efficient technologies each year, leading, however, to more complex operating patterns for the whole system.

Overall, MANGO is a novel contribution to the field of model-based D-MES optimization. With its long-term perspective, it can offer insights that closely match the dynamic class of real-world energy system design projects led by energy developers. It can facilitate strategic decision-making by creating multiple design alternatives that highlight trade-offs between design objectives. Additionally, with its detailed breakdown of costs per year and per expenditure type, it can inform and drive decisions at the economic level. Finally, MANGO generates valuable insights that can assist decisions at the technical engineering levels regarding the design of multiple D-MES in terms of technology selection, sizing and siting, as well as information on the optimal operating patterns of each system.

Future studies should seek to incorporate the issue of uncertainty in the long-term planning of D-MES and extend the model to be able to make robust design decisions considering multiple, possible future scenarios for the dynamic parameters. Additionally, the extension of the end-use sectors considered and the inclusion of mobility applications will enhance the scope and the value that the model can bring to energy developers. Finally, building retrofits in this paper were treated exogenously from the model and only using a set of predefined scenarios. To further enhance retrofit-related decision-making, these decisions could be directly incorporated in the model and their granularity could also be augmented, allowing MANGO to decide, for instance, exactly which building needs to be retrofitted, when and what the optimal intervention should be. This will allow the model to find more globally optimal solutions, balancing between energy retrofit and D-MES solutions.

CRediT authorship contribution statement

Georgios Mavromatidis: Conceptualization, Software, Methodology, Formal analysis, Data curation, Visualization, Writing. **Ivalin Petkov:** Conceptualization, Methodology, Formal analysis, Data curation, Visualization, Writing.

Declaration of competing interest

The authors declare that they have no known competing financial interests or personal relationships that could have appeared to influence the work reported in this paper.

Appendix A. Complete MANGO model formulation

In this appendix, the complete formulation of the novel MANGO (Multi-scAle eNerGy Optimization) model is presented.

A.1. Sets

The model's parameters, variables, and constraints are indexed over the sets described in Table 1. The sets reflect the temporal and spatial dimensions in the model, as well as the considered energy carriers and energy technologies.

A.2. Parameters

The model considers a series of technical, economic, environmental and miscellaneous parameters, which are presented in Tables A.2, A.3, and A.4, respectively. The values for the key model parameters used for this paper's case study are given in Appendix B.

A.2.1. Parameter definitions

Eqs. (A.1) to (A.4) show the definition of model parameters related to performance degradation of conversion and storage technologies and to their salvage value at the end of their lifetime.

$$
\begin{aligned}
cdeg_{c,ec,w,y} = &(1 - cydeg_{c,ec})^{(y-w)}, \\
&\forall\, c \in C,\ ec \in \mathcal{EC},\ w \in \mathcal{W},\ y \in \mathcal{Y}\ | \\
&\{y \geq w \text{ AND } y \leq w + cl_c - 1\}
\end{aligned} \tag{A.1}
$$

$$
\begin{aligned}
sdeg_{s,w,y} = &(1 - sydeg_s)^{(y-w)}, \\
&\forall\, s \in S,\ w \in \mathcal{W},\ y \in \mathcal{Y}\ |\ \{y \geq w \text{ AND } y \leq w + sl_s - 1\}
\end{aligned} \tag{A.2}
$$

$$
\begin{aligned}
cslvg_{c,w} = &\frac{1 - (1+r)^{\max_{y\in\mathcal{Y}}(y)+1-w-cl_c}}{1 - (1+r)^{-cl_c}}, \\
&\forall\, c \in C,\ w \in \mathcal{W}\ |\ \{w \geq \max_{y\in\mathcal{Y}}(y) + 1 - cl_c\}
\end{aligned} \tag{A.3}
$$

$$
\begin{aligned}
sslvg_{s,w} = &\frac{1 - (1+r)^{\max_{y\in\mathcal{Y}}(y)+1-w-sl_s}}{1 - (1+r)^{-sl_s}}, \\
&\forall\, s \in S,\ w \in \mathcal{W}\ |\ \{w \geq \max_{y\in\mathcal{Y}}(y) + 1 - sl_s\}
\end{aligned} \tag{A.4}
$$

A.3. Decision variables

The model's decision variables are presented in Table A.5 and are divided into three key categories. The first category pertains to energy system operation aspects and involves variables representing energy conversion, import, export, exchange and storage. The second category pertains to the design of the energy system and involves variables related to new installations of conversion and storage devices and their capacities, as well as to the diameter and the corresponding cost of thermal interconnections between energy system locations. The third and final category pertains to the economic and environmental performance of the energy system.

A.4. Objective functions

The two most commonly considered objectives are incorporated in the MANGO model. These correspond to the minimization of the lifetime, discounted energy system costs (T^{cost}) and/or CO_2 emissions (T^{CO_2}). The mathematical definitions of the two objective functions are given in Eqs. (A.5) and (A.6), respectively.

$$
\min T^{cost} = \sum_{l,w} \left(C_{l,w}^{INV,TECH} + C_{l,w}^{INV,NET} \right) \cdot \frac{1}{(1+r)^{w-1}}
$$

Table A.2
Technical MANGO model parameters.

Parameter	Unit	Description
Energy conversion technologies		
$\eta^{conv}_{c,ec,w}$	[–]	Conversion factor for technology c and energy carrier ec installed in stage w
$cdeg_{c,ec,w,y}$	[–]	Total degradation coefficient for the conversion factor of technology c and energy carrier ec depending on the installation stage w and the operation year y (Defined for: $\{y \geq w$ and $y \leq w + cl_c - 1\}$)
$cydeg_{c,ec}$	[–]	Yearly degradation coefficient for the conversion factor of technology c and energy carrier ec
cl_c	[years]	Lifetime of conversion technology c
Energy storage technologies		
$stc_{s,ec}$	[–]	Storage technology coupling parameter describing the energy carrier ec stored in storage technology s
η^{ch}_s	[–]	Charging efficiency of storage technology s
η^{dis}_s	[–]	Discharging efficiency of storage technology s
η^{self}_s	[–]	Self-discharge losses of storage technology s
$q^{ch,max}_s$	[–]	Maximum charging rate of storage technology s
$q^{dis,max}_s$	[–]	Maximum discharging rate of storage technology s
$sdeg_{s,w,y}$	[–]	Total degradation coefficient for the charging and discharging efficiencies of storage technology s depending on the installation stage w and the operation year y (Defined for: $\{y \geq w$ and $y \leq w + sl_s - 1\}$)
$sydeg_s$	[–]	Yearly degradation coefficient for the charging and discharging efficiencies of storage technology s
sl_s	[years]	Lifetime of storage technology s
Energy networks		
$\eta^{net}_{ec_x}$	[–]	Losses per meter of network connection transferring energy carrier ec_x
α	[mm/kWh]	Empirical parameter used for the calculation of the necessary pipe diameter for thermal network connections between locations
β	[mm]	Empirical parameter used for the calculation of the necessary pipe diameter for thermal network connections between locations
γ	[CHF/m/mm]	Empirical parameter used for the calculation of the pipe investment cost per meter for thermal network connections between locations
δ	[CHF/m]	Empirical parameter used for the calculation of the pipe investment cost per meter for thermal network connections between locations
Miscellaneous technical parameters		
$dem_{ec_d,l,y,d,t}$	[kWh]	Energy demand for energy carrier ec_d, at location l, in year y, day d and time step t
bio_y	[kWh/m^2]	The available bioenergy (in the form of biomass) per unit of building floor area in year y
$sol_{l,y,d,t}$	[kWh/m^2]	Incoming solar radiation patterns at energy system location l, in year y, day d, and time step t
fa_y	[m^2]	Total building floor area across all energy system locations in year y
$ra_{l,y}$	[m^2]	Total building roof area across at location l, in year y
$x_{l,l'}$	[m]	Distance between energy system locations l and l'
$nd_{y,d}$	[days]	Number of calendar days represented by each representative day d, in year y

Table A.3
Economic MANGO model parameters.

Parameter	Unit	Description
$i_{ec_i,y}$	[CHF/kWh]	Price for importing energy carrier ec_i, in year y
$e_{ec_e,y}$	[CHF/kWh]	Compensation for exporting energy carrier ec_e, in year y
$fc^{conv}_{c,w}$	[CHF]	Fixed cost for the installation of conversion technology c, in investment stage w
$lc^{conv}_{c,w}$	[CHF/kW]	Linear, capacity-dependent cost for the installation of conversion technology c, in investment stage w
$fc^{stor}_{s,w}$	[CHF]	Fixed cost for the installation of storage technology s, in investment stage w
$lc^{stor}_{s,w}$	[CHF/kWh]	Linear, capacity-dependent cost for the installation of storage technology s, in investment stage w
om^{conv}_c	[–]	Parameter used to calculate the annual maintenance cost for conversion technology c as a fraction of its total investment cost
om^{stor}_s	[–]	Parameter used to calculate the annual maintenance cost for storage technology s as a fraction of its total investment cost
$cslvg_{c,w}$	[–]	Salvage percentage of initial investment cost for conversion technology c that was installed in stage w and has not reached the end of its lifetime at the end of the model horizon (Defined for: $\{w \geq \max_{y \in \mathcal{Y}}(y) + 1 - cl_c\}$)
$sslvg_{s,w}$	[–]	Salvage percentage of initial investment cost for storage technology s that was installed in stage w and has not reached the end of its lifetime at the end of the model horizon (Defined for: $\{w \geq \max_{y \in \mathcal{Y}}(y) + 1 - sl_s\}$)
r	[–]	Discount rate

$$+ \sum_{l,y} \left(C^{IMP}_{l,y} + C^{MAINT}_{l,y} \right) \cdot \frac{1}{(1+r)^y}$$

$$- \sum_{l,y} R^{EXP}_{l,y} \cdot \frac{1}{(1+r)^y} - \sum_l R^{SLVG}_l \cdot \frac{1}{(1+r)^{|\mathcal{Y}|+1}} \tag{A.5}$$

$$\min T^{CO_2} = \sum_{ec_i,d,t} \left(P^{imp}_{ec_i,l,y,d,t} \cdot c_{ec_i,y} \cdot nd_{y,d} \right) \tag{A.6}$$

The T^{cost} objective is composed of summation terms including the investment costs for energy technologies ($C^{INV,TECH}_{l,w}$) and network technologies ($C^{INV,NET}_{l,w}$) at each location l and investment stage w,

Table A.4
Environmental and miscellaneous MANGO model parameters.

Parameter	Unit	Description
$bigM$	[–]	"Big M" - Sufficiently large value
$c_{ec_i,y}$	[kgCO$_2$/kWh]	Carbon emission factor for imported energy carrier ec_i in year y

the energy carrier import costs ($C_{l,y}^{IMP}$), maintenance costs ($C_{l,y}^{MAINT}$) and revenues due to energy carrier exports ($B_{l,y}^{EXP}$) at each location l and calendar year y, and, finally, the salvage value at each site w at the end of the model horizon due to technologies not reaching the end of their lifetime (R_l^{SLVG}). Definitions for these terms are given in Eqs. (A.7) to (A.12).[12]

Note that all cost terms are discounted to present value using the discount rate r. Cost terms pertaining to investment expenditure are assumed to occur at the beginning of the investment stage/year, hence, the exponent $w - 1$ in the discounting term of Eqs. (A.7) and (A.8). The same applies to the salvage revenue term (B_l^{SLVG}) with the discounting term using the term $|\mathcal{Y}| - 1$ as the exponent ($|\mathcal{Y}|$ denotes the cardinality of the set $\mathcal{Y}$, which in this case refers to the number of years considered). On the other hand, operating expenditures are assumed to occur at the end of the calendar year, so the exponent of the discounting term is only y in Eqs. (A.9) to (A.11).

$$C_{l,w}^{INV,TECH} = \sum_c \left[lc_{c,w}^{conv} \cdot NCAP_{c,l,w}^{conv} + fc_{c,w}^{conv} \cdot Y_{c,l,w}^{conv} \right]$$
$$+ \sum_s \left[lc_{s,w}^{stor} \cdot NCAP_{s,l,w}^{stor} + fc_{s,w}^{stor} \cdot Y_{s,l,w}^{stor} \right], \quad \text{(A.7)}$$
$$\forall l \in \mathcal{L}, \ w \in \mathcal{W}$$

$$C_{l,w}^{INV,NET} = \sum_{\substack{l' \\ l' \neq l}} \left[Y_{ec_x,l,l',w}^{net} \cdot LC_{l,l'}^{net} \cdot x_{l,l'} \cdot 0.5 \right],$$
$$\forall ec_x = Heat, l \in \mathcal{L}, \ w \in \mathcal{W} \quad \text{(A.8)}$$

$$C_{l,y}^{IMP} = \sum_{ec_i,d,t} \left[P_{ec_i,l,y,d,t}^{imp} \cdot i_{ec_i,y} \cdot nd_{y,d} \right], \ \forall l \in \mathcal{L}, \ y \in \mathcal{Y} \quad \text{(A.9)}$$

$$C_{l,y}^{MAINT} = \sum_{\substack{c,w \\ y \geq w \\ y \leq w+cl_c-1}} \left[lc_{c,w}^{conv} \cdot NCAP_{c,l,w}^{conv} + fc_{c,w}^{conv} \cdot Y_{c,l,w}^{conv} \right] \cdot om_c^{conv}$$
$$+ \sum_{\substack{s,w \\ y \geq w \\ y \leq w+sl_s-1}} \left[lc_{s,w}^{stor} \cdot NCAP_{s,l,w}^{stor} + fc_{s,w}^{stor} \cdot Y_{s,l,w}^{stor} \right] \cdot om_s^{stor}, \quad \text{(A.10)}$$
$$\forall l \in \mathcal{L}, \ y \in \mathcal{Y}$$

$$R_{l,y}^{EXP} = \sum_{ec_e,d,t} \left[P_{ec_e,l,y,d,t}^{exp} \cdot e_{ec_e,y} \cdot nd_{y,d} \right], \ \forall l \in \mathcal{L}, \ y \in \mathcal{Y} \quad \text{(A.11)}$$

$$R_l^{SLVG} = \sum_{\substack{c,w \\ w \geq |\mathcal{Y}|-cl_c+1}} \left[lc_{c,w}^{conv} \cdot NCAP_{c,l,w}^{conv} + fc_{c,w}^{conv} \cdot Y_{c,l,w}^{conv} \right] \cdot cslvg_{c,w}$$
$$+ \sum_{\substack{c,w \\ w \geq |\mathcal{Y}|-sl_s+1}} \left[lc_{s,w}^{stor} \cdot NCAP_{s,l,w}^{stor} + fc_{s,w}^{stor} \cdot Y_{s,l,w}^{stor} \right] \cdot sslvg_{c,w}, \quad \text{(A.12)}$$
$$\forall l \in \mathcal{L}$$

---

[12] The 0.5 term in Eq. (A.8) is added to attribute equally the network costs to both interconnected sites.

A.5. Constraints

A.5.1. Energy balances

The constraint in Eq. (A.13) describes how the energy demands of the end-users at the different locations are met at each time step of the model via energy imports, energy conversion, conversion, energy storage charging and discharging, energy exchanges, while also allowing for energy exports.

$$dem_{ec_d,l,y,d,t} = P_{ec_i,l,y,d,t}^{imp} + \sum_{\substack{c,w \\ y \geq w \\ y \leq w+cl_c-1}} \left(P_{c,l,w,y,d,t}^{conv} \cdot \eta_{c,ec,w}^{conv} \cdot cdeg_{c,ec,w,y} \right)$$
$$+ \sum_{\substack{s,w \\ y \geq w \\ y \leq w+sl_s-1}} \left[stc_{s,ec} \cdot (Q_{s,l,w,y,d,t}^{dis} - Q_{s,l,w,y,d,t}^{ch}) \right]$$
$$+ \sum_{\substack{l,l' \\ l \neq l'}} \left[P_{ec_x,l',l,y,d,t}^{exc} \cdot (1 - \eta_{ec_x}^{net} \cdot x_{l',l}) - P_{ec_x,l,l',y,d,t}^{exc} \right] - P_{ec_e,l,y,d,t}^{exp},$$
$$\forall ec \in \mathcal{EC}, \ l \in \mathcal{L}, \ y \in \mathcal{Y}, \ d \in \mathcal{D}, \ t \in \mathcal{T}$$

(A.13)

A.5.2. Conversion technology constraints

Eq. (A.14) prevents the violation of the nominal capacities of conversion technologies during the system's operation.

$$NCAP_{c_d,l,w}^{conv} \geq P_{c_d,l,w,y,d,t}^{conv} \cdot \eta_{c_d,ec,w}^{conv} \cdot cdeg_{c_d,ec,w,y},$$
$$\forall c_d \in C_d, ec \in \mathcal{EC}, l \in \mathcal{L}, \ w \in \mathcal{W}, \ y \in \mathcal{Y}, \ d \in \mathcal{D}, \ t \in \mathcal{T} \mid$$
$$\{y \geq w \text{ AND } y \leq w+cl_{c_d}-1 \text{ AND } \eta_{c_d,ec,w}^{conv} > 0\}$$

(A.14)

Eq. (A.15) defines the input energy to solar energy technologies as the product of the incoming solar radiation multiplied by the installed capacity of the technology.

$$P_{c_s,l,w,y,d,t}^{conv} = sol_{l,y,d,t} \cdot NCAP_{c_s,l,w}^{conv}$$
$$\forall c_s \in C_s, ec \in \mathcal{EC}, l \in \mathcal{L}, \ w \in \mathcal{W}, \ y \in \mathcal{Y}, \ d \in \mathcal{D}, \ t \in \mathcal{T} \mid$$
$$\{y \geq w \text{ AND } y \leq w+cl_{c_s}-1\}$$

(A.15)

Eq. (A.16) states that the total installed capacity of solar energy technologies in each year and location cannot exceed the available roof area.

$$\sum_{\substack{c_s,w \\ y \geq w \\ y \leq w+cl_{c_{sol}}-1}} NCAP_{c_{sol},l,w}^{conv} \leq ra_{l,y}, \ \forall y \in \mathcal{Y}, \ l \in \mathcal{L} \quad \text{(A.16)}$$

Eq. (A.17) limits the total annual consumption of biomass across all sites to account for biomass availability. In this work, the value for the parameter bio_y is calculated by dividing the estimated domestic biomass potential for Switzerland from [57] with the yearly projected total building floor areas for the country from [54].

$$\sum_{\substack{ec_i,s,d,t \\ ec_i = Biomass}} P_{ec_i,l,d,t}^{imp} \cdot nd_{y,d} \leq bio_y \cdot fa_y, \ \forall y \in \mathcal{Y} \quad \text{(A.17)}$$

Eq. (A.18) is a Big-M constraint that forces binary variable $Y_{c,l,w}^{conv}$ to be equal to 1, if the variable $NCAP_{c,l,w}^{conv}$ gets a non-zero value.

$$NCAP_{c,l,w}^{conv} \leq bigM \cdot Y_{c,l,w}^{conv}, \ \forall c \in C, \ l \in \mathcal{L}, \ w \in \mathcal{W} \quad \text{(A.18)}$$

A.5.3. Storage technology constraints

Eqs. (A.19) and (A.20) describe the energy balances of each storage technology and, more specifically, the relationship between a technology's state of charge and charging and discharging energy flows. Additionally, the influence of performance degradation is included via the term $sdeg_{s,w,y}$. The need for two equations to describe the storage energy balances stems from the use of a set of typical days to represent

Table A.5
MANGO model decision variables.

Parameter	Unit	Description
Energy system operation		
$P^{conv}_{c,l,w,y,d,t}$	[kWh]	Input energy to conversion technology c, installed at energy system location l, in investment stage w, and operating in year y, day d, and time step t (Defined for: $\{y \geq w$ and $y \leq w + cl_c - 1\}$)
$P^{imp}_{ec_i,l,y,d,t}$	[kWh]	Import of energy carrier ec_i, at energy system location l, in year y, day d, and time step t
$P^{exp}_{ec_e,l,y,d,t}$	[kWh]	Exported energy of energy carrier ec_e, at energy system location l, in year y, day d, and time step t
$P^{exc}_{ec_x,l,l',y,d,t}$	[kWh]	Exchanged energy of energy carrier ec_x, from location l to location l', in year y, day d, and time step t (Defined for: $\{l \neq l'\}$)
$Q^{ch}_{s,l,w,y,d,t}$	[kWh]	Charging energy for storage technology s, installed at energy system location l, in investment stage w, and operating in year y, day d, and time step t
$Q^{dis}_{s,l,w,y,d,t}$	[kWh]	Discharging energy for storage technology s, installed at energy system location l, in investment stage w, and operating in year y, day d, and time step t
$SoC_{s,l,w,y,d,t}$	[kWh]	State of charge of storage technology s, installed at energy system location l, in investment stage w, and operating in year y, day d, and time step t
Energy system design		
$NCAP^{conv}_{c,l,w}$	[kW, m^2]	New capacity of conversion technology c, installed at location l, in investment stage w
$NCAP^{strg}_{s,l,w}$	[kWh]	New capacity of storage technology s, installed at location l, in investment stage w
$Y^{conv}_{c,l,w}$	[–]	Binary variable denoting the installation of new capacity of conversion technology c, at location l, in investment stage w
$Y^{strg}_{s,l,w}$	[–]	Binary variable denoting the installation of new capacity of storage technology s, at location l, in investment stage w
$dm_{l,l'}$	[mm]	Pipe diameter for thermal connections between energy system locations l, l' (Defined for: $\{l \neq l'\}$)
$LC^{net}_{l,l'}$	[CHF/m]	Interconnection cost to exchange energy carrier ec_x between locations l,l' (Defined for: $\{l \neq l'\}$)
$Y^{net}_{ec_x,l,l',w}$	[–]	Binary variable denoting the initial connection to exchange energy carrier ec_x, between energy system locations l, l', in investment stage w (Defined for: $\{l \neq l'\}$)
Energy system cost and emission performance		
T^{cost}	[CHF]	Total lifetime energy system cost
T^{CO_2}	[kgCO$_2$]	Total lifetime energy system CO$_2$ emissions
$C^{IMP}_{l,y}$	[CHF]	Total cost due to energy carrier imports at location l, in year y
$C^{MAINT}_{l,y}$	[CHF]	Total maintenance cost for all conversion and storage technologies installed at location l, in year y
$C^{INV,TECH}_{l,w}$	[CHF]	Total investment cost for conversion and storage technologies at location l, in investment stage w
$C^{INV,NET}_{l,w}$	[CHF]	Total investment cost for network technologies at location l, in investment stage w
$R^{EXP}_{l,y}$	[CHF]	Total income due to energy carrier exports at location l, in year y
R^{SLVG}_{l}	[CHF]	Salvage value of all conversion and storage technologies at location l not reaching the end of their lifetime at the end of the model horizon

each modeled year, which means that the continuity between the days is no longer valid. As a result, the storage devices are assumed to only be able to cover daily demand and production fluctuations. Therefore, Eq. (A.19) applies to all time steps of a typical day except for the first one. In this case, Eq. (A.20) applies, which

$$
\begin{aligned}
SoC_{s,l,w,y,d,t} =& \left((1 - \eta_s^{self}) \cdot SoC_{s,l,w,y,d,t-1} \right) + \left(Q^{ch}_{s,l,w,y,d,t} \cdot \eta_s^{ch} \cdot sdeg_{s,w,y} \right) \\
& - \left(Q^{dis}_{s,l,w,y,d,t} \cdot \frac{1}{\eta_s^{dis} \cdot sdeg_{s,w,y}} \right), \\
& \forall\, s \in S,\ l \in \mathcal{L},\ w \in \mathcal{W}, \\
& y \in \mathcal{Y},\ d \in \mathcal{D},\ t \in \mathcal{T}\ | \\
& \{y \geq w \text{ AND } y \leq w + sl_s - 1 \text{ AND } t \neq 1\}
\end{aligned}
$$
(A.19)

$$
\begin{aligned}
SoC_{s,l,w,y,d,t} =& \left((1 - \eta_s^{self}) \cdot SoC_{s,l,w,y,d,t+|\mathcal{T}|-1} \right) \\
& + \left(Q^{ch}_{s,l,w,y,d,t} \cdot \eta_s^{ch} \cdot sdeg_{s,w,y} \right) \\
& - \left(Q^{dis}_{s,l,w,y,d,t} \cdot \frac{1}{\eta_s^{dis} \cdot sdeg_{s,w,y}} \right), \\
& \forall\, s \in S,\ l \in \mathcal{L},\ w \in \mathcal{W}, \\
& y \in \mathcal{Y},\ d \in \mathcal{D},\ t \in \mathcal{T}\ | \\
& \{y \geq w \text{ AND } y \leq w + sl_s - 1 \text{ AND } t = 1\}
\end{aligned}
$$
(A.20)

Eqs. (A.21) and (A.22) limit the maximum charge and discharge rates as a function of the installed capacity of a storage technology.

$$
Q^{ch}_{s,l,w,y,d,t} \leq q^{ch,max}_s \cdot NCAP^{stor}_{s,l,w},
$$
$$
\forall\, s \in S,\ l \in \mathcal{L},\ w \in \mathcal{W},\ y \in \mathcal{Y},\ d \in \mathcal{D},\ t \in \mathcal{T}
$$
(A.21)

$$
Q^{dis}_{s,l,w,y,d,t} \leq q^{dis,max}_s \cdot NCAP^{stor}_{s,l,w},
$$
$$
\forall\, s \in S,\ l \in \mathcal{L},\ w \in \mathcal{W},\ y \in \mathcal{Y},\ d \in \mathcal{D},\ t \in \mathcal{T}
$$
(A.22)

Eq. (A.23) states that the state of charge of a storage technology cannot exceed its rated capacity.

$$
SoC_{s,l,w,y,d,t} \leq NCAP^{stor}_{s,l,w},
$$
$$
\forall\, s \in S,\ l \in \mathcal{L},\ w \in \mathcal{W},\ y \in \mathcal{Y},\ d \in \mathcal{D},\ t \in \mathcal{T}\ |
$$
$$
\{y \geq w \text{ AND } y \leq w + sl_s - 1\}
$$
(A.23)

Eq. (A.24) is a Big-M constraint that forces binary variable $Y^{stor}_{s,l,w}$ to be equal to 1, if the variable $NCAP^{stor}_{s,l,w}$ gets a non-zero value.

$$
NCAP^{stor}_{s,l,w} \leq bigM \cdot Y^{stor}_{s,l,w},\ \forall s \in S,\ l \in \mathcal{L},\ w \in \mathcal{W}
$$
(A.24)

A.5.4. Network technology and energy exchange constraints

Another collection of model constraints pertains to the interconnections between energy systems at different locations, their characteristics and the exchanged energy.

More specifically, Eq. (A.25) specifies that the initial connection can only occur once during the project horizon, while Eq. (A.26) specifies that this connection is bidirectional. Eq. (A.27) is a big-M constraint that allows energy to be exchanged between two locations only if a connection between them already exists.

$$\sum_w Y^{net}_{ec_x,l,l',w} \leq 1 \ , \ \forall \ ec_x \in \mathcal{EC}_x, \ l,l' \in \mathcal{L} \mid l \neq l' \tag{A.25}$$

$$Y^{net}_{ec_x,l,l',w} = Y^{net}_{ec_x,l',l,w} \ , \ \forall \ ec_x \in \mathcal{EC}_x, \ l,l' \in \mathcal{L}, \ w \in \mathcal{W} \mid l \neq l' \tag{A.26}$$

$$P^{exc}_{ec_x,l,l',y,d,t} \leq bigM \cdot \sum_{\substack{w \\ w \leq y}} Y^{net}_{ec_x,l,l',w} \ ,$$
$$\forall \ ec_x \in \mathcal{EC}_x, \ l,l' \in \mathcal{L}, \ y \in \mathcal{Y}, \ d \in \mathcal{D}, \ t \in \mathcal{T} \mid l \neq l' \tag{A.27}$$

Eq. (A.28) is a constraint that is used for the calculation of the necessary pipe diameter for the thermal interconnection between two energy system locations.

$$dm_{l,l'} \geq \alpha \cdot P^{exc}_{ec_x,l,l',y,d,t} + \beta \cdot \sum_w Y^{net}_{ec_x,l,l',w} \ ,$$
$$\forall \ ec_x = \text{Heat}, \ l,l' \in \mathcal{L}, \ y \in \mathcal{Y}, \ d \in \mathcal{D}, \ t \in \mathcal{T} \mid l \neq l' \tag{A.28}$$

Eq. (A.29) is a constraint that is used for the calculation of the necessary pipe diameter for the thermal interconnection between two energy system locations.

$$dm_{l,l'} = dm_{l',l} \ , \ \forall \ l,l' \in \mathcal{L} \mid l \neq l' \tag{A.29}$$

Eq. (A.30), finally, is used to calculate the piping cost per meter of network connection as a function of the pipe diameter.

$$LC^{net}_{l,l'} = \gamma \cdot dm_{l,l'} + \delta \cdot \sum_w Y^{net}_{ec_x,l,l',w} \ , \ \forall \ ec_x = \text{Heat}, \ l,l' \in \mathcal{L} \mid l \neq l'$$
$$\tag{A.30}$$

As can be seen from these network constraints, in addition to Eq. (A.13), the networks in the MANGO are modeled in a simplified way, considering only distance-dependent losses when energy is exchanged. Since MANGO is mostly concerned with planning decisions and not detailed network performance considerations, this choice was made for the sake of computational efficiency. Nevertheless, more advanced approaches to represent thermal and electrical networks in MILP models can be found in [58] and [59], respectively.

Appendix B. Model parameter values used for the case study

In this appendix, the values for the most relevant model parameters are reported in Tables B.6 to B.10. The discount rate, r, used in the analysis is taken as equal to 5%.

Further data not explicitly provided in the manuscript, for instance regarding the values of the multi-year energy demand and renewable availability time series, will be made available to anyone upon reasonable request.

Appendix C. Further case study results

See Figs. C.17–C.19.

Table B.6

Energy carrier import prices and export compensation, along with the CO_2 emission factor for grid electricity during the 30-year planning horizon. All price and compensation units are in CHF/kWh and the CO_2 emission factor in $kgCO_2$/kWh. Ref. [53] is used to obtain the current (2021) values for the import prices and export compensation. Ref. [55] is used to obtain the current (2021) value for the grid emission factor. Ref. [54] is used to create the projections for all values according to the NEP scenario.

	Import prices			Export compensation	CO$_2$ emission factors
Ref.	[53,54]	[53,54]	[53,54]	[53,54]	[54,55]
Year	Natural gas, $i_{gas,y}$	Biomass, $i_{bio,y}$	Grid electricity, $i_{elec,y}$	Grid electricity, $e_{elec,y}$	Grid electricity, $c_{elec,y}$
2021	0.073	0.072	0.159	0.053	0.024
2022	0.074	0.074	0.161	0.054	0.028
2023	0.075	0.076	0.163	0.054	0.031
2024	0.076	0.079	0.165	0.055	0.035
2025	0.077	0.081	0.166	0.055	0.038
2026	0.079	0.085	0.169	0.056	0.042
2027	0.081	0.089	0.171	0.057	0.046
2028	0.083	0.093	0.173	0.058	0.050
2029	0.084	0.096	0.175	0.058	0.053
2030	0.086	0.100	0.177	0.059	0.057
2031	0.087	0.103	0.179	0.060	0.071
2032	0.089	0.106	0.181	0.060	0.085
2033	0.090	0.108	0.183	0.061	0.099
2034	0.091	0.111	0.184	0.061	0.112
2035	0.093	0.114	0.186	0.062	0.126
2036	0.094	0.116	0.186	0.062	0.121
2037	0.094	0.118	0.187	0.062	0.115
2038	0.095	0.120	0.187	0.062	0.110
2039	0.096	0.122	0.187	0.062	0.104
2040	0.097	0.124	0.187	0.062	0.098
2041	0.098	0.125	0.188	0.063	0.094
2042	0.098	0.126	0.189	0.063	0.089
2043	0.099	0.128	0.190	0.063	0.084
2044	0.100	0.129	0.191	0.064	0.079
2045	0.100	0.130	0.193	0.064	0.074
2046	0.101	0.131	0.193	0.064	0.069
2047	0.101	0.133	0.193	0.064	0.064
2048	0.102	0.134	0.194	0.065	0.059
2049	0.103	0.135	0.194	0.065	0.054
2050	0.103	0.136	0.195	0.065	0.049

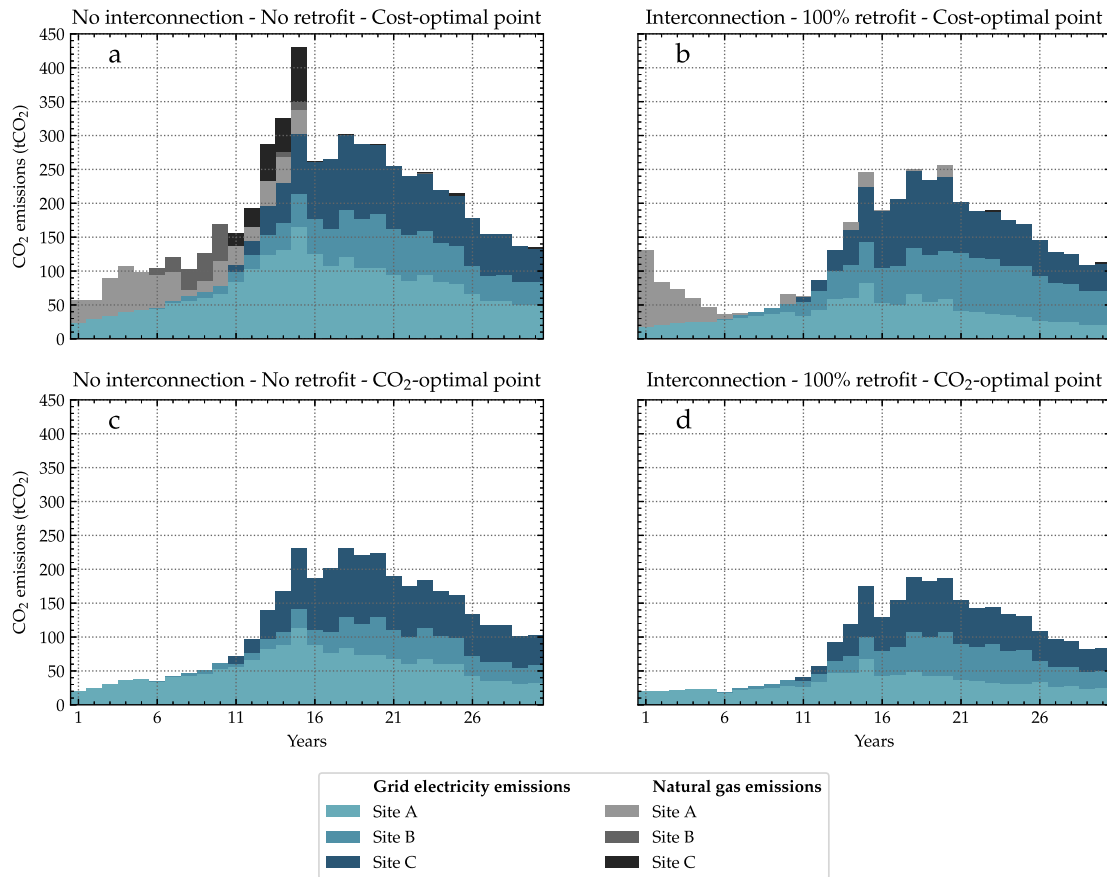**Fig. C.17.** CO$_2$ emissions over the 30-year planning period for two interconnection–retrofit scenarios and for the cost- and CO$_2$-optimal Pareto points.
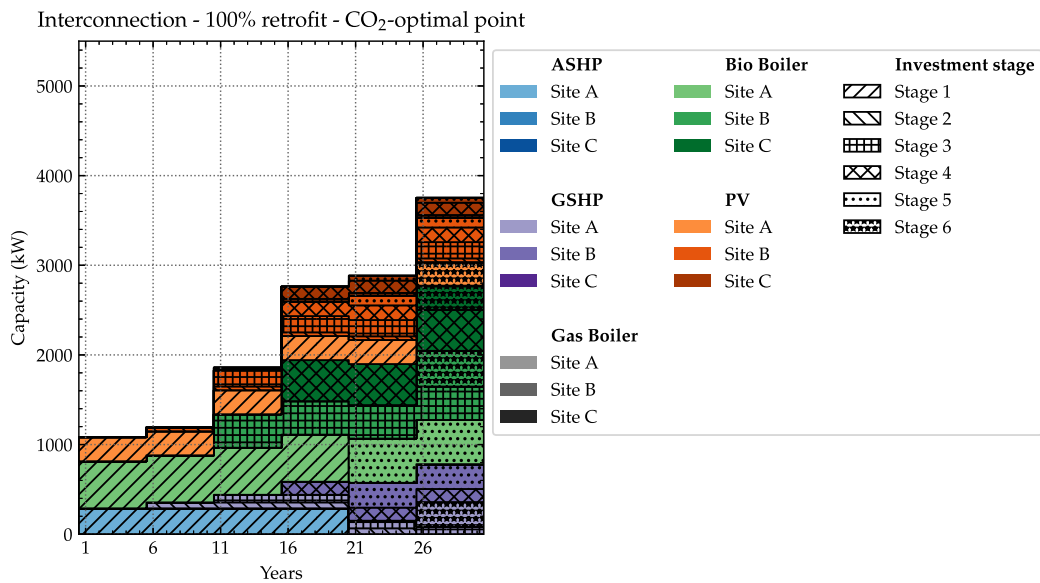

Fig. C.18. Visualization of installed capacities of energy conversion technologies at each site and each Investment stage during the 30-year planning period for the 'Interconnection - 100% retrofit' scenario and the CO$_2$-optimal Pareto point.

Table B.7

Dynamic cost (fixed and linear) and efficiency coefficients of GSHP, ASHP, PV, and Battery technologies during the 30-year planning horizon based on the learning curve coefficient (μ) for each technology. $C_y = C_o \cdot e^{-\mu y}$. All fixed cost ($fc$) units are in CHF, while all linear cost (lc) units are in CHF/kW for the GSHP, ASHP and CHP, in CHF/m^2 for PV, and in CHF/kWh for the Battery. In the Table, references labeled with $*$ are used to obtain current (2021) cost values and efficiencies for the technologies, while references labeled with $+$ are used to create projections for the future.

	GSHP			ASHP			CHP		PV			Battery
μ	0.035			0.027			0.005		0.021			0.019
Ref.	[60]*, [61]+	[60]*, [61]+	[62]*,+, [63]*,+	[60]*, [61]+	[60]*, [61]+	[62]*,+, [63]*,+	[64]*,+	[64]*,+	[22]+, [64]*	[22]+, [64]*	[22]*, [65]+	[22]*,+, [66]+, [67]+
Year	$fc^{conv}_{GSHP,w}$	$lc^{conv}_{GSHP,w}$	$\eta^{conv}_{GSHP,w}$	$fc^{conv}_{ASHP,w}$	$lc^{conv}_{ASHP,w}$	$\eta^{conv}_{ASHP,w}$	$fc^{conv}_{CHP,w}$	$lc^{conv}_{CHP,w}$	$fc^{conv}_{PV,w}$	$lc^{conv}_{PV,w}$	$\eta^{conv}_{PV,w}$	$lc^{stor}_{BAT,w}$
2021	49,130	2450	4.00	49,635	610	3.00	63,280	790	17,610	115	17.0%	235
2022	47,440	2366	4.04	48,313	594	3.03	62,964	786	17,250	113	17.2%	231
2023	45,809	2284	4.08	47,026	578	3.06	62,650	782	16,897	110	17.3%	227
2024	44,233	2206	4.12	45,773	563	3.09	62,338	778	16,551	108	17.5%	222
2025	42,712	2130	4.17	44,554	548	3.12	62,027	774	16,212	106	17.7%	218
2026	41,243	2057	4.21	43,367	533	3.16	61,718	770	15,880	104	17.9%	214
2027	39,824	1986	4.25	42,212	519	3.19	61,410	767	15,555	102	18.0%	210
2028	38,454	1918	4.29	41,087	505	3.22	61,104	763	15,237	100	18.2%	206
2029	37,132	1852	4.33	39,993	491	3.25	60,799	759	14,925	97	18.4%	202
2030	35,855	1788	4.37	38,927	478	3.28	60,496	755	14,620	95	18.6%	198
2031	34,621	1726	4.41	37,890	466	3.31	60,194	751	14,321	94	18.7%	195
2032	33,431	1667	4.46	36,881	453	3.34	59,894	748	14,028	92	18.9%	191
2033	32,281	1610	4.50	35,899	441	3.37	59,595	744	13,741	90	19.1%	188
2034	31,170	1554	4.54	34,942	429	3.40	59,298	740	13,459	88	19.2%	184
2035	30,098	1501	4.58	34,011	418	3.43	59,002	737	13,184	86	19.4%	181
2036	29,063	1449	4.62	33,105	407	3.47	58,078	733	12,914	84	19.6%	177
2037	28,064	1399	4.66	32,224	396	3.50	58,415	729	12,650	83	19.8%	174
2038	27,098	1351	4.70	31,365	385	3.53	58,123	726	12,391	81	19.9%	171
2039	26,166	1305	4.74	30,530	375	3.56	57,834	722	12,137	79	20.1%	167
2040	25,266	1260	4.79	29,716	365	3.59	57,545	718	11,889	78	20.3%	164
2041	24,397	1217	4.83	28,925	355	3.62	57,258	715	11,646	76	20.4%	161
2042	23,558	1175	4.87	28,154	346	3.65	56,973	711	11,407	74	20.6%	158
2043	22,748	1134	4.91	27,404	337	3.68	56,588	708	11,174	73	20.8%	155
2044	21,965	1095	4.95	26,674	328	3.71	56,406	704	10,945	71	21.0%	152
2045	21,210	1058	4.99	25,964	319	3.74	56,124	701	10,721	70	21.1%	149
2046	20,480	1021	5.03	25,272	311	3.78	55,844	697	10,502	69	21.3%	147
2047	19,776	986	5.08	24,599	302	3.81	55,566	694	10,287	67	21.5%	144
2048	19,096	952	5.12	23,943	294	3.84	55,289	690	10,076	66	21.7%	141
2049	18,439	920	5.16	23,306	286	3.87	55,013	687	9870	64	21.8%	139
2050	17,805	888	5.20	22,685	279	3.90	54,739	683	9668	63	22.0%	136

Table B.8

Constant costs (fixed and linear), conversion efficiency, lifetime, degradation, and O&M cost coefficients of all conversion technologies. Where there are missing values (–), parameters change over the 30-year planning horizon (see Table B.7).

Technical characteristic	GSHP	ASHP	Natural gas boiler	Biomass boiler	CHP	PV
Fixed conversion technology cost, $fc^{conv}_{c,w}$ (CHF)	–	–	23,785 [60]	55,885 [60]	–	–
Linear conversion technology cost, $lc^{conv}_{c,w}$ (CHF/kW)	–	–	175 [60]	320 [60]	–	–
Conversion factor, $\eta^{conv}_{c,ec,w}$	–	–	90% [68]	85% [21]	55% (thermal) [21] 35% (electrical) [21]	–
Conversion technology lifetime, cl_c (years)	20 [21]	20 [22]	20 [21]	20 [21]	20 [21]	25 [69]
Yearly conversion degradation coefficient, $cydeg_c$	2.0% [70]	2.0% [70]	1.0% [70]	1.0% [70]	2.0% [71]	0.5% [72]
Maintenance cost factor, om^{conv}_c	1.5% [18]	1.5% [18]	2.0% [73]	2.0% [73]	1.5% [18]	1.5% [6]

Table B.9

Constant techno-economic characteristics of thermal and the battery electrical storage technologies.

Technical characteristic	Thermal	Battery
Charge/discharge efficiency, η^{ch}_s/η^{dis}_s	90% [74]	90% [21]
Maximum charge/discharge rate, $q^{ch,max}_s/q^{dis,max}_s$	25% [74]	25% [22]
Self-discharge rate, η^{self}_s	0.50% [18]	0.06% [75]
Fixed storage technology cost, $fc^{stor}_{s,w}$ (CHF)	1685 [21]	–
Linear storage technology cost, $lc^{stor}_{s,w}$ (CHF/kWh)	13 [21]	–
Storage technology lifetime, sl_s (years)	30 [76]	15 [77]
Yearly storage degradation coefficient, $sydeg_s$	0%	2.0% [78,79]
Maintenance cost factor, om^{stor}_s	2.0% [18]	2.0% [18]

Table B.10

Technical characteristics of network technologies.

| Technical characteristic	Value
Thermal network efficiency, η^{net}_s/η^{heat}	98.2% [80]
Electrical network efficiency, η^{net}_s/η^{heat}	99.8% [80]
Empirical parameter for pipe diameter calculation, α	0.073 [81]
Empirical parameter for pipe diameter calculation, β	32.2 [81]
Empirical parameter for pipe investment cost per meter calculation, γ	6.49 [81]
Empirical parameter for pipe investment cost per meter calculation, δ	168.4 [81]
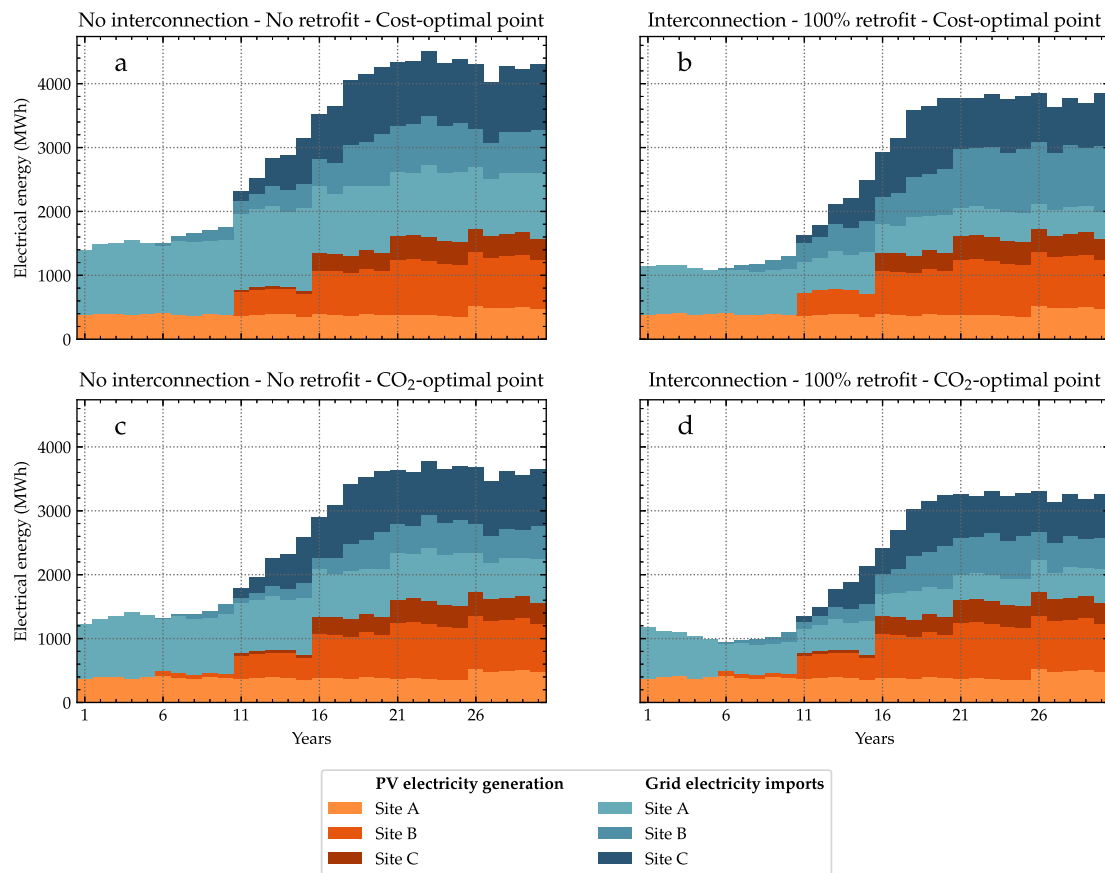
Fig. C.19. Evolution of local electricity generation and grid electricity imports at each site during the 30-year planning period for two interconnection–retrofit scenarios and for the cost- and CO_2-optimal Pareto points.

References

[1] REN21. Renewables in cities 2019 global status report, paris, REN21 secretariat. Tech. rep., Paris; 2019, URL https://www.ren21.net/reports/cities-global-status-report/.

[2] International Energy Agency. Energy technology perspectives 2016: Towards sustainable urban energy systems. Energy technology perspectives, OECD; 2016, http://dx.doi.org/10.1787/energy_tech-2016-en.

[3] Good N, Martínez Ceseña EA, Zhang L, Mancarella P. Techno-economic and business case assessment of low carbon technologies in distributed multi-energy systems. Appl Energy 2016;167:158–72. http://dx.doi.org/10.1016/j.apenergy.2015.09.089.

[4] Sepponen M, Heimonen I. Business concepts for districts' energy hub systems with maximised share of renewable energy. Energy Build 2016;124:273–80. http://dx.doi.org/10.1016/j.enbuild.2015.07.066.

[5] Mavromatidis G, Orehounig K, Bollinger LA, Hohmann M, Marquant JF, Miglani S, Morvaj B, Murray P, Waibel C, Wang D, Carmeliet J. Ten questions concerning modeling of distributed multi-energy systems. Build Environ 2019;165:106372. http://dx.doi.org/10.1016/j.buildenv.2019.106372.

[6] Grosspietsch D, Thömmes P, Girod B, Hoffmann VH. How, when, and where? assessing renewable energy self-sufficiency at the neighborhood level. Environ Sci Technol 2018;52(4):2339–48. http://dx.doi.org/10.1021/acs.est.7b02686.

[7] Zhang X, Lovati M, Vigna I, Widén J, Han M, Gal C, Feng T. A review of urban energy systems at building cluster level incorporating renewable-energy-source (RES) envelope solutions. Appl Energy 2018;230:1034–56. http://dx.doi.org/10.1016/j.apenergy.2018.09.041.

[8] Braslavsky JH, Wall JR, Reedman LJ. Optimal distributed energy resources and the cost of reduced greenhouse gas emissions in a large retail shopping centre. Appl Energy 2015;155:120–30. http://dx.doi.org/10.1016/j.apenergy.2015.05.085.

[9] Mashayekh S, Stadler M, Cardoso G, Heleno M. A mixed integer linear programming approach for optimal DER portfolio, sizing, and placement in multi-energy microgrids. Appl Energy 2017;187:154–68. http://dx.doi.org/10.1016/j.apenergy.2016.11.020.

[10] Petkov I, Gabrielli P. Power-to-hydrogen as seasonal energy storage: An uncertainty analysis for optimal design of low-carbon multi-energy systems. Appl Energy 2020;274:115197. http://dx.doi.org/10.1016/j.apenergy.2020.115197.

[11] Mavromatidis G, Orehounig K, Carmeliet J. Climate change impact on the design of urban energy systems. In: Proceedings of international conference cisbat 2015: future buildings and districts sustainability from nano to urban scale. Lausanne, LESO-PB, EPFL; 2015, http://dx.doi.org/10.5075/EPFL-CISBAT2015-853-858.

[12] McKenna R, Fehrenbach D, Merkel E. The role of seasonal thermal energy storage in increasing renewable heating shares: A techno-economic analysis for a typical residential district. Energy Build 2019;187:38–49. http://dx.doi.org/10.1016/j.enbuild.2019.01.044.

[13] Orehounig K, Evins R, Dorer V. Integration of decentralized energy systems in neighbourhoods using the energy hub approach. Appl Energy 2015;154:277–89. http://dx.doi.org/10.1016/j.apenergy.2015.04.114.

[14] Murray P, Carmeliet J, Orehounig K. Multi-objective optimisation of power-to-mobility in decentralised multi-energy systems. Energy 2020;205:117792. http://dx.doi.org/10.1016/j.energy.2020.117792.

[15] Ramos-Teodoro J, Rodríguez F, Berenguel M, Torres JL. Heterogeneous resource management in energy hubs with self-consumption: contributions and application example. Appl Energy 2018;229:537–50. http://dx.doi.org/10.1016/j.apenergy.2018.08.007.

[16] Comodi G, Bartolini A, Carducci F, Nagaranjan B, Romagnoli A. Achieving low carbon local energy communities in hot climates by exploiting networks synergies in multi energy systems. Appl Energy 2019;256:113901. http://dx.doi.org/10.1016/j.apenergy.2019.113901.

[17] Kotzur L, Markewitz P, Robinius M, Stolten D. Time series aggregation for energy system design: modeling seasonal storage. Appl Energy 2018;213:123–35. http://dx.doi.org/10.1016/j.apenergy.2018.01.023.

[18] Gabrielli P, Gazzani M, Martelli E, Mazzotti M. Optimal design of multi-energy systems with seasonal storage. Appl Energy 2018;219:408–24. http://dx.doi.org/10.1016/j.apenergy.2017.07.142.

[19] Waibel C, Evins R, Carmeliet J. Co-simulation and optimization of building geometry and multi-energy systems: interdependencies in energy supply, energy demand and solar potentials. Appl Energy 2019;242:1661–82. http://dx.doi.org/10.1016/j.apenergy.2019.03.177.

[20] Baumgärtner N, Delorme R, Hennen M, Bardow A. Design of low-carbon utility systems: exploiting time-dependent grid emissions for climate-friendly demand-side management. Appl Energy 2019;247:755–65. http://dx.doi.org/10.1016/j.apenergy.2019.04.029.

[21] Mavromatidis G, Orehounig K, Carmeliet J. Uncertainty and global sensitivity analysis for the optimal design of distributed energy systems. Appl Energy 2018;214:219–38. http://dx.doi.org/10.1016/j.apenergy.2018.01.062.

[22] Murray P, Orehounig K, Grosspietsch D, Carmeliet J. A comparison of storage systems in neighbourhood decentralized energy system applications from 2015 to 2050. Appl Energy 2018;231:1285–306. http://dx.doi.org/10.1016/j.apenergy.2018.08.106.

[23] Loulou R, Labriet M. ETSAP-TIAM: The TIMES integrated assessment model. part I: model structure. Comput Manag Sci 2008;5(1–2):7–40. http://dx.doi.org/10.1007/s10287-007-0046-z.

[24] Loulou R. ETSAP-TIAM: The TIMES integrated assessment model. part II: Mathematical formulation. Comput Manag Sci 2008;5(1–2):41–66. http://dx.doi.org/10.1007/s10287-007-0045-0.

[25] IEA-ETSAP. Overview of TIMES modelling tool. 2020, URL https://iea-etsap.org/index.php/etsap-tools/model-generators/times.

[26] Howells M, Rogner H, Strachan N, Heaps C, Huntington H, Kypreos S, Hughes A, Silveira S, DeCarolis J, Bazillian M, Roehrl A. OSeMOSYS: the open source energy modeling system: an introduction to its ethos, structure and development. Energy Policy 2011;39(10):5850–70. http://dx.doi.org/10.1016/j.enpol.2011.06.033.

[27] Marquant JF, Evins R, Bollinger LA, Carmeliet J. A holarchic approach for multi-scale distributed energy system optimisation. Appl Energy 2017;208:935–53. http://dx.doi.org/10.1016/j.apenergy.2017.09.057.

[28] Yazdanie M, Densing M, Wokaun A. The role of decentralized generation and storage technologies in future energy systems planning for a rural agglomeration in Switzerland. Energy Policy 2016;96:432–45. http://dx.doi.org/10.1016/j.enpol.2016.06.010.

[29] Yazdanie M, Densing M, Wokaun A. Cost optimal urban energy systems planning in the context of national energy policies: A case study for the city of basel. Energy Policy 2017;110:176–90. http://dx.doi.org/10.1016/j.enpol.2017.08.009.

[30] Cano EL, Groissböock M, Moguerza JM, Stadler M. A strategic optimization model for energy systems planning. Energy Build 2014;81:416–23. http://dx.doi.org/10.1016/j.enbuild.2014.06.030.

[31] Pecenak ZK, Stadler M, Fahy K. Efficient multi-year economic energy planning in microgrids. Appl Energy 2019;255:113771. http://dx.doi.org/10.1016/j.apenergy.2019.113771.

[32] Wei J, Zhang Y, Wang J, Cao X, Khan MA. Multi-period planning of multi-energy microgrid with multi-type uncertainties using chance constrained information gap decision method. Appl Energy 2020;260:114188. http://dx.doi.org/10.1016/j.apenergy.2019.114188.

[33] Faraji J, Hashemi-Dezaki H, Ketabi A. Multi-year load growth-based optimal planning of grid-connected microgrid considering long-term load demand forecasting: A case study of Tehran, Iran. Sustain Energy Technol Assess 2020;42:100827. http://dx.doi.org/10.1016/j.seta.2020.100827.

[34] HOMER. HOMER Pro - Microgrid Software for Designing Optimized Hybrid Microgrids. HOMER Energy LLC; 2020, URL https://www.homerenergy.com/products/pro/index.html.

[35] Grinold RC. Time horizons in energy planning models. In: Ziemba WT, Schwartz SL, editors. Energy policy modeling: United States and Canadian experiences. Dordrecht: Springer Netherlands; 1980, p. 216–32. http://dx.doi.org/10.1007/978-94-009-8751-7_12.

[36] Maroufmashat A, Elkamel A, Fowler M, Sattari S, Roshandel R, Hajimiragha A, Walker S, Entchev E. Modeling and optimization of a network of energy hubs to improve economic and emission considerations. Energy 2015;93:2546–58. http://dx.doi.org/10.1016/j.energy.2015.10.079.

[37] Keirstead J, Samsatli N, Shah N, Weber C. The impact of CHP (combined heat and power) planning restrictions on the efficiency of urban energy systems. Energy 2012;41(1):93–103. http://dx.doi.org/10.1016/j.energy.2011.06.011.

[38] Gurobi Optimization LLC. Gurobi optimizer reference manual. 2020, URL https://www.gurobi.com/documentation/.

[39] IBM ILOG CPLEX Division. IBM CPLEX Optimizer. 2020, URL https://www.ibm.com/analytics/cplex-optimizer.

[40] Østergaard PA. Reviewing optimisation criteria for energy systems analyses of renewable energy integration. Energy 2009;34(9):1236–45. http://dx.doi.org/10.1016/j.energy.2009.05.004.

[41] Iqbal M, Azam M, Naeem M, Khwaja A, Anpalagan A. Optimization classification, algorithms and tools for renewable energy: A review. Renew Sustain Energy Rev 2014;39:640–54. http://dx.doi.org/10.1016/j.rser.2014.07.120.

[42] Mavrotas G. Effective implementation of the ε-constraint method in multi-objective mathematical programming problems. Appl Math Comput 2009;213(2):455–65. http://dx.doi.org/10.1016/j.amc.2009.03.037.

[43] Birge JR, Louveaux F. Introduction to stochastic programming. Springer series in operations research and financial engineering, second ed.. New York: Springer; 2011.

[44] Mavromatidis G, Orehounig K, Carmeliet J. Design of distributed energy systems under uncertainty: A two-stage stochastic programming approach. Appl Energy 2018;222:932–50. http://dx.doi.org/10.1016/j.apenergy.2018.04.019.

[45] Zug Estates. Sustainability report 2018 - Suurstoffi energy system. Tech. rep., 2018, p. 1–60, URL https://www.zugestates.ch/fileadmin/user_upload/redakteure/pdf/nachhaltigkeitsberichte/ZugEstates_Sustainability_Report_2018_en.pdf.

[46] Meuer J, Lamaro F, Vetterli N. Embedding energy optimization in organizations: a case study of a swiss decentralized renewable energy system. Energy and Buildings 2021;235:110710. http://dx.doi.org/10.1016/j.enbuild.2020.110710.

[47] Mavromatidis G. Model-based design of distributed urban energy systems under uncertainty (Doctoral Thesis), ETH Zurich; 2017, http://dx.doi.org/10.3929/ethz-b-000182697.

[48] Murray P, Marquant J, Niffeler M, Mavromatidis G, Orehounig K. Optimal transformation strategies for buildings, neighbourhoods and districts to reach CO_2 emission reduction targets. Energy Build 2020;207:109569. http://dx.doi.org/10.1016/j.enbuild.2019.109569.

[49] EnergyPlus. EnergyPlus simulation software. 2019, URL https://energyplus.net/.

[50] SIA. SIA 380/1 - Heizwärmebedarf. SIA - Swiss Society of Engineers and Architects; 2016.

[51] Domínguez-Muñoz F, Cejudo-López JM, Carrillo-Andrés A, Gallardo-Salazar M. Selection of typical demand days for CHP optimization. Energy Build 2011;43(11):3036–43. http://dx.doi.org/10.1016/j.enbuild.2011.07.024.

[52] Schütz T, Schraven MH, Fuchs M, Remmen P, Müller D. Comparison of clustering algorithms for the selection of typical demand days for energy system synthesis. Renew Energy 2018;129:570–82. http://dx.doi.org/10.1016/j.renene.2018.06.028.

[53] SFOE. Schweizerische Gesamtenergiestatistik 2018. Tech. rep., Swiss Federal Office of Energy (SFOE); 2019, URL https://www.bfe.admin.ch/bfe/en/home/supply/statistics-and-geodata/energy-statistics/overall-energy-statistics.html.

[54] Prognos AG. Die energieperspektiven fur die schweiz bis 2050. Tech. rep., Swiss Federal Office of Energy (SFOE); 2012, URL https://www.bfe.admin.ch/bfe/en/home/policy/energy-strategy-2050/documentation/energy-perspectives-2050.html.

[55] BFE EnDK and EnFK. Harmonisiertes fördermodell der kantone HFM 2015. Tech. rep., 2015, URL https://www.endk.ch/de/dokumentation/harmonisiertes-foerdermodell-der-kantone-hfm.

[56] Swiss Federal Office of Energy. Federal council decides to gradually phase out nuclear energy as part of its new energy strategy. 2011.

[57] Steubing B, Zah R, Waeger P, Ludwig C. Bioenergy in Switzerland: assessing the domestic sustainable biomass potential. Renew Sustain Energy Rev 2010;14(8):2256–65. http://dx.doi.org/10.1016/j.rser.2010.03.036.

[58] van der Heijde B, Aertgeerts A, Helsen L. Modelling steady-state thermal behaviour of double thermal network pipes. Int J Therm Sci 2017;117:316–27. http://dx.doi.org/10.1016/j.ijthermalsci.2017.03.026.

[59] Morvaj B, Evins R, Carmeliet J. Optimization framework for distributed energy systems with integrated electrical grid constraints. Appl Energy 2016;171:296–313. http://dx.doi.org/10.1016/j.apenergy.2016.03.090.

[60] HSLU. Heizkostenvergleichsrechner. luzern: hochschule luzern (HSLU). 2019, URL https://www.hslu.ch/de-ch/technik-architektur/forschung/kompetenzzentren/zig/software-tools/.

[61] Danish Energy Agency and Energinet. Technology Data for Individual Heating 2016. Tech. rep., Danish Energy Agency and Energinet; 2018, p. 1–167, URL https://ens.dk/en/our-services/projections-and-models/technology-data/technology-data-individual-heating-plants.

[62] David A, Mathiesen BV, Averfalk H, Werner S, Lund H. Heat roadmap europe: large-scale electric heat pumps in district heating systems. Energies 2017;10(4):578. http://dx.doi.org/10.3390/en10040578.

[63] Coujard C, Peirano E, Sanchis G, Betraoui B. e-HIGHWAY 2050: Modular development plan of the pan-European transmission system 2050. Tech. rep., EU; 2013, p. 1–16, URL https://docs.entsoe.eu/baltic-conf/bites/www.e-highway2050.eu/fileadmin/documents/Results/D3/report_heat_pumps.pdf.

[64] SCCER JASM. Energy conversion technologies in STEM. 2020, Available from: https://data.sccer-jasm.ch/energy-conversion-technologies-stem/2020-03-05/.

[65] Polman A, Knight M, Garnett EC, Ehrler B, Sinke WC. Photovoltaic materials: present efficiencies and future challenges. Science 2016;352(6283). http://dx.doi.org/10.1126/science.aad4424.

[66] Nykvist B, Nilsson M. Rapidly falling costs of battery packs for electric vehicles. Nature Clim Change 2015;5(4):329–32. http://dx.doi.org/10.1038/nclimate2564.

[67] IRENA. Electricity storage and renewables: Costs and markets to 2030. Tech. rep., International Renewable Energy Agency; 2017, p. 1–132, URL http://www.climateaction.org/images/uploads/documents/IRENA_Electricity_Storage_Costs_2017.pdf.

[68] Di Somma M, Yan B, Bianco N, Graditi G, Luh PB, Mongibello L, Naso V. Multi-objective design optimization of distributed energy systems through cost and exergy assessments. Appl Energy 2017;204:1299–316. http://dx.doi.org/10.1016/j.apenergy.2017.03.105.

[69] Kurtz S. Reliability and durability of PV modules. In: Reinders A, Verlinden P, van Sark W, Freundlich A, editors. Photovoltaic solar energy. Chichester, UK: John Wiley & Sons, Ltd; 2017, p. 491–501. http://dx.doi.org/10.1002/9781118927496.ch44.

[70] Eleftheriadis G, Hamdy M. The impact of insulation and HVAC degradation on overall building energy performance: a case study. Buildings 2018;8(2):23. http://dx.doi.org/10.3390/buildings8020023.

[71] Lee JH, Kim TS, Kim E-h. Prediction of power generation capacity of a gas turbine combined cycle cogeneration plant. Energy 2017;124:187–97. http://dx.doi.org/10.1016/j.energy.2017.02.032.

[72] Jordan DC, Kurtz SR. Photovoltaic degradation rates – an analytical review. Tech. rep., National Renewable Energy Laboratory; 2012, p. 1–32, URL https://www.nrel.gov/docs/fy12osti/51664.pdf.

[73] Sandvall AF, Ahlgren EO, Ekvall T. Cost-efficiency of urban heating strategies – modelling scale effects of low-energy building heat supply. Energy Strateg Rev 2017;18:212–23. http://dx.doi.org/10.1016/j.esr.2017.10.003.

[74] Stadler M, Groissböck M, Cardoso G, Marnay C. Optimizing distributed energy resources and building retrofits with the strategic DER-camodel. Appl Energy 2014;132:557–67. http://dx.doi.org/10.1016/j.apenergy.2014.07.041.

[75] Gabrielli P, Fürer F, Mavromatidis G, Mazzotti M. Robust and optimal design of multi-energy systems with seasonal storage through uncertainty analysis. Appl Energy 2019;238:1192–210. http://dx.doi.org/10.1016/j.apenergy.2019.01.064.

[76] Bracco S, Dentici G, Siri S. DESOD: A mathematical programming tool to optimally design a distributed energy system. Energy 2016;100:298–309. http://dx.doi.org/10.1016/j.energy.2016.01.050.

[77] DiOrio N, Dobos A, Janzou S. Economic analysis case studies of battery energy storage with SAM. Tech. rep., National Renewable Energy Laboratory; 2015, p. 1–22, URL https://www.nrel.gov/docs/fy16osti/64987.pdf.

[78] Stroe D-I, Knap V, Swierczynski M, Stroe A-I, Teodorescu R. Operation of a grid-connected lithium-ion battery energy storage system for primary frequency regulation: a battery lifetime perspective. IEEE Trans Ind Appl 2017;53(1):430–8. http://dx.doi.org/10.1109/TIA.2016.2616319.

[79] Swierczynski M, Stroe DI, Laerke R, Stan AI, Kjaer PC, Teodorescu R, Kaer SK. Field experience from li-ion BESS delivering primary frequency regulation in the danish energy market. ECS Trans 2014;61(37):1–14. http://dx.doi.org/10.1149/06137.0001ecst.

[80] Mehleri ED, Sarimveis H, Markatos NC, Papageorgiou LG. A mathematical programming approach for optimal design of distributed energy systems at the neighbourhood level. Energy 2012;44(1):96–104. http://dx.doi.org/10.1016/j.energy.2012.02.009.

[81] Nussbaumer T, Thalmann S. Influence of system design on heat distribution costs in district heating. Energy 2016;101:496–505. http://dx.doi.org/10.1016/j.energy.2016.02.062.